GEOLOGY OF THE INTERMOUNTAIN WEST
an open-access journal of the Utah Geological Association
ISSN 2380-7601

Volume 8 ***2021***

CARBONATE MOUND SPRINGS OF THE UPPER JURASSIC MORRISON FORMATION OF CENTRAL MONTANA AND THEIR PALEOCLIMATIC SIGNIFICANCE FOR THE NORTHERN FORELAND BASIN

Dean R. Richmond, John Pigott, Richard Lupia, Michael Behm, and David Hein

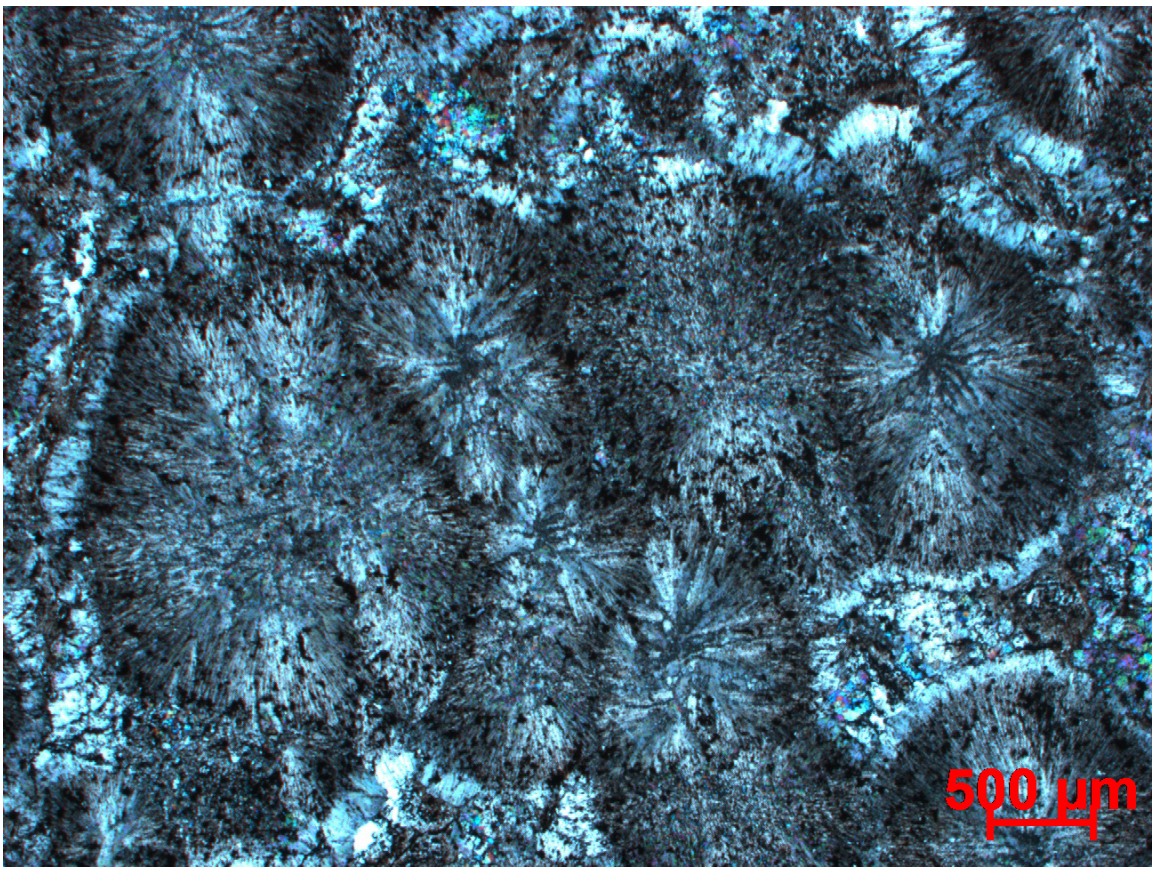

GEOLOGY OF THE INTERMOUNTAIN WEST

an open-access journal of the Utah Geological Association

ISSN 2380-7601

Volume 8 ***2021***

Editors

Douglas A. Sprinkel
Azteca Geosolutions
801.391.1977
GIW@utahgeology.org
dsprinkel@gmail.com

Bart J. Kowallis
Brigham Young University
801.380.2736
bkowallis@gmail.com

Steven Schamel
GeoX Consulting, Inc.
801.583-1146
geox-slc@comcast.net

Thomas C. Chidsey, Jr.
Utah Geological Survey
801.824.0738
tomchidsey@gmail.com

John R. Foster
Utah Field House of
Natural History State Park
Museum
435.789.3799
eutretauranosuchus@
gmail.com

Production

Cover Design and Desktop Publishing
Douglas A. Sprinkel

Cover

Photomicrograph of carbonate spherulites formed by a Jurassic variant of the betaproteobacteria ***Ralstonia eutropha*** *H16. The spherulites are commonly found in the upper surfaces of mound spring deposits of the Upper Jurassic Morrison Formation of central Montana. The black specks are interpreted to be fossil betaproteobacteria remnants preserved in the spherulite. Image shown in crossed nicols.*

2020–2021 UGA Board

President	Riley Brinkerhoff	riley.brinkerhoff@gmail.com	406.839.1375
President-Elect	John South	john.south@dominionenergy.com	385.266.2113
Program Chair	Maria Slack	petromns18@gmail.com	801.810.9154
Treasurer	Brent Greenhalgh	brent.greenhalgh@dominionenergy.com	385.626.8972
Secretary	Ryan Gall	rgall@utah.gov	801.537.3312
Past President	Leslie Heppler	lheppler@utah.gov	801.538.5257

UGA Committees

Environmental Affairs	Craig Eaton	eaton@ihi-env.com	801.633.9396
Geologic Road Sign	Greg Gavin	greg@loughlinwater.com	801.541.6258
Historian	Paul Anderson	paul@pbageo.com	801.364.6613
Membership	Rick Ford	rford@weber.edu	801.626.6942
Outreach	Greg Nielsen	gnielsen@weber.edu	801.626.6394
Public Education	Zach Anderson	zanderson@utah.gov	801.537.3300
	Matt Affolter	gfl247@yahoo.com	
Publications	Paul Inkenbrandt	paulinkenbrandt@utah.gov	801.537.3361
Publicity	Paul Inkenbrandt	paulinkenbrandt@utah.gov	801.537.3361
Social/Recreation	Roger Bon	rogerbon@xmission.com	801.942.0533

AAPG House of Delegates

2020–2023 Term	David A. Wavrek	dwavrek@petroleumsystems.com	801.322.2915

State Mapping Advisory Committee

UGA Representative	Bill Loughlin	bill@loughlinwater.com	435.649.4005

Earthquake Safety Committee

Chair	Grant Willis	gwillis@utah.gov	801.537.3355

UGA Website — www.utahgeology.org

Webmaster	Paul Inkenbrandt	paulinkenbrandt@utah.gov	801.537.3361

UGA Newsletter

Newsletter Editor	Bill Lund	uga.newsletter@gmail.com	435.590.1338

Become a member of the UGA to help support the work of the Association and receive notices for monthly meetings, annual field conferences, and new publications. Annual membership is $20 and annual student membership is only $5. Visit the UGA website at www.utahgeology.org for information and membership application.

The UGA board is elected annually by a voting process through UGA members. However, the UGA is a volunteer-driven organization, and we welcome your voluntary service. If you would like to participate please contact the current president or committee member corresponding with the area in which you would like to volunteer.

Utah Geological Association formed in 1970 from a merger of the Utah Geological Society, founded in 1946, and the Intermountain Association of Geologists, founded in 1949. Affiliated with the American Association of Petroleum Geologists.

GEOLOGY OF THE INTERMOUNTAIN WEST
an open-access journal of the Utah Geological Association
Volume 8 ***2021***

Carbonate Mound Springs of the Upper Jurassic Morrison Formation of Central Montana and Their Paleoclimatic Significance for the Northern Foreland Basin

Dean R. Richmond[1], John Pigott[1], Richard Lupia[2], Michael Behm[1], and David Hein[3]
[1]School of Geosciences, University of Oklahoma, Sarkeys Energy Center Suite 710, Norman, OK 73019, USA; drichmaond.ou.edu; jpigott@ou.edu; Michael.Behm@geodata.com
[2]Sam Noble Museum, University of Oklahoma, 2401 Chautauqua Avenue, Norman, OK 73072, USA; rlupia@ou.edu
[3]1021 Toole Circle, Billings, MT 59105, USA

ABSTRACT

Recent investigations of the Upper Jurassic Morrison Formation in central Montana resulted in the discovery of 105 small (< 3 m diameter) carbonate buildups in close geographic and stratigraphic proximity. The buildups are divided into two groups by dominant mineralogic composition: siderite versus calcium carbonate. The buildups are found in five distinct spatial clusters and are distributed in association with, and in alignment to, regional Jurassic-aged structural lineaments. The buildups are distributed stratigraphically between 40 to 52 m above the base of the Morrison Formation. Interpretation of electrical resistivity tomography surveys indicates that additional buildups are present in the subsurface. Carbonate-rich groundwater migrated up fractures to the capillary fringe or the surface. The siderite buildups formed in the near subsurface capillary fringe, whereas the carbonate mounds are subartesian mound spring tufa deposits. The bulk rock negative $\delta^{18}O$ and $\delta^{13}C$ values demonstrate the buildups were produced by meteoric waters in a continental setting with the groundwater having a short residence time in the subsurface. The presence of the subsurface buildups and mound spring tufa deposits scattered throughout a 12-m portion of the Morrison section indicates that the region experienced extended periods of increased precipitation.

INTRODUCTION

The Upper Jurassic Morrison Formation, an expansive sequence of terrestrial sediments deposited in foreland basins formed by the North America Cordilleran orogenic system, covers approximately 1.5 million km^2 of the Intermountain West (Dodson and others, 1980). The formation has been intensely studied for uranium (Turner-Peterson and Fishman, 1986), coal (Harris, 1966; Silverman and Harris, 1966), oil and gas (Johnson, 2005), and dinosaurs (Foster 2007). Jurassic dinosaurs have been discovered in every U.S. state where the Morrison Formation is exposed (Turner and Peterson, 1999). Age equivalent rocks are found in south-central Canada but have only yielded plant fossils; vertebrate fossils have yet to be discovered (Brown, 1946; Rouse, 1959; Jansa, 1972).

The recent discovery of dinosaurs in the northernmost portion of the Morrison foreland basin prompted a geological investigation of the study area that led to the discovery of numerous strange hemisphere-shaped terrestrial carbonate mounds (Richmond and

Citation for this article.
Richmond, D.R., Pigott, J., Lupia, R., Behm, M., and Hein, D., 2021, Carbonate mound springs of the Upper Jurassic Morrison Formation of central Montana and their paleoclimatic significance for the northern foreland basin: Geology of the Intermountain West, v. 8, p. 1–26, https://doi.org/10.31711/giw.v8.pp1-26.

others, 2020). These are the first terrestrial carbonate mounds for the Morrison Formation. The purpose of this paper is to document the surface and near-subsurface spatial configuration of the buildups, place them into a stratigraphic framework, compare them to other terrestrial carbonates and draw conclusions as to the environmental conditions that led to their development, and understand their paleoclimatic significance.

GEOLOGIC SETTING

The study area is in southeastern Fergus County, Montana, where the Morrison Formation is exposed along the flanks of the Spindletop Dome (figure 1). Based on field stratigraphic measurements and well log data, the Morrison Formation in the study area is 72 m in thickness. The formation is bounded by the underlying Upper Jurassic Swift Formation and the overlying Lower Cretaceous Kootenai Formation. In central Montana, the Morrison Formation is conformable with the underlying marine sandstone beds of the Swift Formation. The J-5 unconformity (Pipiringos and O'Sullivan, 1978), present at the base of the Morrison Formation in more southern states, is absent in central Montana (this study; Imlay, 1954; Uhlir and others, 1988; Khalid, 1990; Meyers and Schwartz, 1994; Fuentes and others, 2011). The Morrison Formation is undifferentiated in central Montana and consists of a mudstone-dominated section with fine-grained anastomosing fluvial channels and thin crevasse splay sandstone beds (Richmond and Murphy, 2020). The formation contains fossil invertebrates (Richmond and others, 2017), dinosaurs (Saitta, 2015; Richmond and Murphy, 2017), and fossil wood (Richmond and others, 2019a, 2019b, 2019c). The overlying Lower Cretaceous (Aptian) Kootenai Formation rests on the K-1 unconformity and is an alluvial and fluvial sequence comprised of deposits of coarse- to medium-grained fluvial sandstone beds, overbank deposits of mudstone, and calcrete paleosols, with the formation capped by interstratified lacustrine limestone and dolomite units (Dupree, 2009).

There is a hypothetical relationship between the structural components of central Montana and the development of the Morrison carbonate buildups, therefore a summary of the structural features of the region is presented. The present-day structure of the

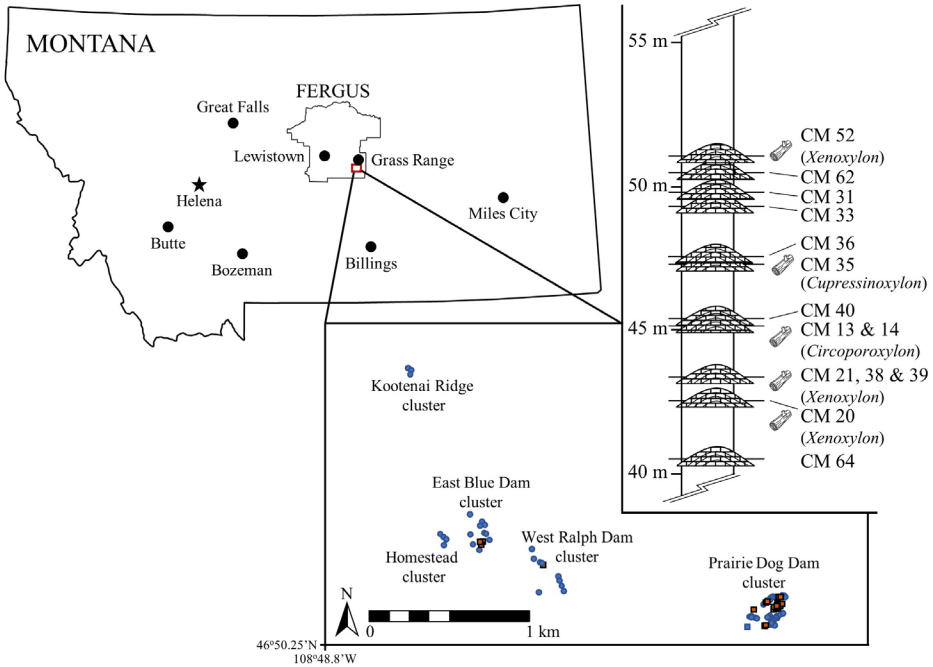

Figure 1. Geographic distribution for carbonate (blue circles) and siderite (orange squares) buildups in southeastern Fergus County, Montana. The buildups are separated into five different clusters. Only a sample of the 105 buildups is represented in the stratigraphic section. Some of the carbonate mounds have associated fossil wood, as indicated. Height in the stratigraphic section is reported in meters above the conformable Swift/Morrison formational contact.

central Montana region is complex (Porter and others, 2002) as verified by fracture swarms and compressional and extensional faulting. The structure of central Montana, and the majority of the state, is related to Precambrian laterally extensive basement faults that trend at approximately 50° azimuth from southwestern to northeastern Montana (Sims and others, 2004). Reactivation of these Precambrian zones of crustal weakness during the Laramide orogenic event of the Late Cretaceous and Early Paleogene likely formed many of the present-day structures of central Montana, including the anticlinal structures of the Big and Little Snowy Mountains, Spindletop Dome, Flat Willow, and the Cat Creek anticlines and many other local anticlinal features (Gardner, 1950). There are two major orthogonal lineaments present in the Montana Rocky Mountains and the adjacent plains (Maughan, 1993). The northeast-southwest lineaments (Great Falls, Greenhorn, Snake River-Yellowstone, and Greybull) strike between 45° to 50° azimuth and correlate to the Precambrian basement faults. The major northwest-southeast lineaments (Bridger, Chadron, and Cedar Creek) strike between 320° to 325° azimuth, (Maughan, 1993; figure 2). In central Montana, this broad zone of northeast-southwest-trending structures controlled depositional patterns for some Paleozoic and Mesozoic sedimentary rocks (O'Neill and Lopez, 1993). Steeply dipping basement faults that strike northeast-southwest and southeast-northwest in Fergus, Petroleum, and Garfield Counties have been mapped in central Montana and are thought to have been reactivated through geologic time (Nelson, 1995).

During the Late Jurassic, Sevier orogenic thrusting formed large north-trending folds in southwestern Montana (Hutsinpiller and Parry, 1985). A paleogeographic/paleotectonic high called "Belt Island" in north-central Montana (Porter, 2011) was likely the result of Jurassic reactivation of Precambrian basement faults in the plate interior. However, there are no known plutonic emplacements in central Montana related to these Jurassic regional paleostresses. The earliest granitic plutonism occurred during the Late Cretaceous between 74 and 69 Ma in west-central Montana in the Big and Little Belt Mountains (Snee and others, 2002).

METHODS

Geological Data Collection

Stratigraphic measurements were made using accepted geological methods and surveyed using a Nikon DTM-322 total station. Samples retrieved were thin sectioned by Wagner Petrographic (Lindon, Utah) and subsequently were examined under a Zeiss petrographic microscope. The spatial position of each buildup was determined by a handheld Garmin GPS. The buildups appear to have a linear component to

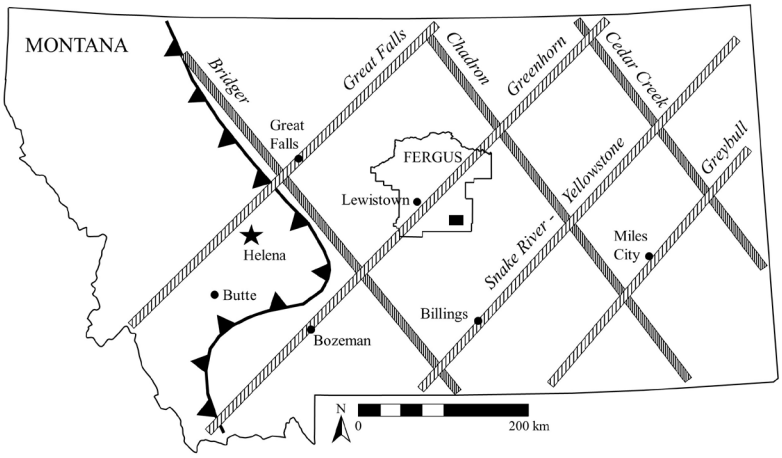

Figure 2. Regional stress lineaments for the central Rocky Mountains have a prolonged geologic history. The latest reactivation occurred during the Laramide orogenic event. The major northwest-southeast lineaments (Bridger, Chadron, and Cedar Creek) strike between 320° to 325° azimuth, whereas the northeast-southwest lineaments (Great Falls, Greenhorn, Snake River-Yellowstone, and Greybull) strike between 45° to 50° azimuth. The lineaments are an important component of the development of the Morrison Formation carbonate mounds. The small black rectangle in southeastern Fergus County indicates the study area. Modified from Maughan (1993).

them, therefore best fit lines were drawn for the spatial latitude and longitude data.

Geochemical Analysis

Carbonate samples were prepared for X-ray diffraction (XRD) with accepted methods (Moore and Reynolds, 1997). Powder XRD analyses were performed at the University of Oklahoma School of Geosciences using a Rigaku Ultima IV diffractometer. Cu-K-alpha radiation (40 kV, 44 mA) was used with a scintillation detector. Data analysis was completed using Jade 2010 software with the International Centre for Diffraction Data PDF4+ database.

A Thermo Scientific Niton XL3t Ultra Analyzer X-ray fluorescence (XRF) gun was used to measure the elemental abundance of the carbonates. The device measured each sample for 210 seconds. Forty-one elements were measured using the XRF tool; 28 of these elements provide useful insight into the rock's mineralogic composition. Only the highest percentages of elements are shown for this study.

Isotopic Data Collection

Two siderite and fourteen carbonate mounds and the modern cascade tufa from Sitting Bull Falls, (Last Chance Canyon, New Mexico), were sampled for standard isotopic data. A single sample was analyzed from each mound and the Sitting Bull Falls tufa. The 17 samples were analyzed by Beta Lab Services in Houston Texas. Three duplicate samples (CM 13, CM 35, and CM 52) were also analyzed at the Stable Isotope Geoscience Facilities at Texas A&M University. All isotope values are reported in delta notation relative to the Vienna Pee Dee Belemnite (VPDB‰) isotopic standard.

Geophysical Data Collection

Electrical resistivity tomography (ERT) data were acquired using an ARES-II system with stainless steel electrodes at a 1-m and 2-m spacing. All four profiles were measured using a dipole electrode configuration, sensitive to both lateral and vertical changes in resistivity. The ERT data were processed and inverted using AGI EarthImagerTM 2D resistivity inversion and modeling software. Overall, a relatively moderate to low data misfit (< 6%) was achieved after removing data outliers with a small number of iterations. Challenges do arise in interpreting ERT measurements when pronounced heterogeneity resulting from varying fracture density, karstification, or thin layering occurs below the resolution threshold (e.g., Everett, 2013; Loke and others, 2013). Furthermore, electrical resistivity is largely governed by water content within the soil profile and greatly depends on the primary and secondary porosity of the rocks and soil.

MORRISON FORMATION BUILDUPS

The Morrison Formation buildups can be separated into five geographic distinct areas designated by local coulee dams or other surface features (figure 3). The names of the clusters moving west to east: Kootenai Ridge cluster (46°51'10.45"N., 108°48'33.03"W.), Homestead cluster (46°50'36.50"N., 108°48'21.86"W.), East Blue Dam cluster (46°50'37.61"N., 108°48'12.21"W.), West Ralph Dam cluster (46°50'31.10"N., 108°47'50.94"W.), and Prairie Dog Dam cluster (46°50'23.67"N., 108°46'46.52"W.). The Prairie Dog Dam cluster has the highest number of siderite and carbonate buildups (figure 3).

The buildups are stratigraphically between 40 to 52 m above the base of the Morrison Formation. The majority of the buildups are small hemisphere-shaped features a meter in height above the ground surface elevation and up to 3 m in diameter. The buildups are divided into two classes: siderite ($FeCO_3$) and carbonate ($CaCO_3$) buildups. To distinguish between the two types of buildups, they will be referred to as siderite buildups (SB) and carbonate mounds (CM). At present, 34 siderite buildups and 71 carbonate mounds have been discovered. The buildups and mounds occur in 5 clusters and 10 carbonate mounds have fossil wood associated with them. All buildups and mounds are encased in variegated illitic or organic-rich mudstones with no associated fluvial or lacustrine facies. Some of the designated carbonate mounds have siderite present beneath and on the flanks of the mound. The contact between the siderite and carbonate is always sharp and distinct where these siderite-carbonate mounds occur.

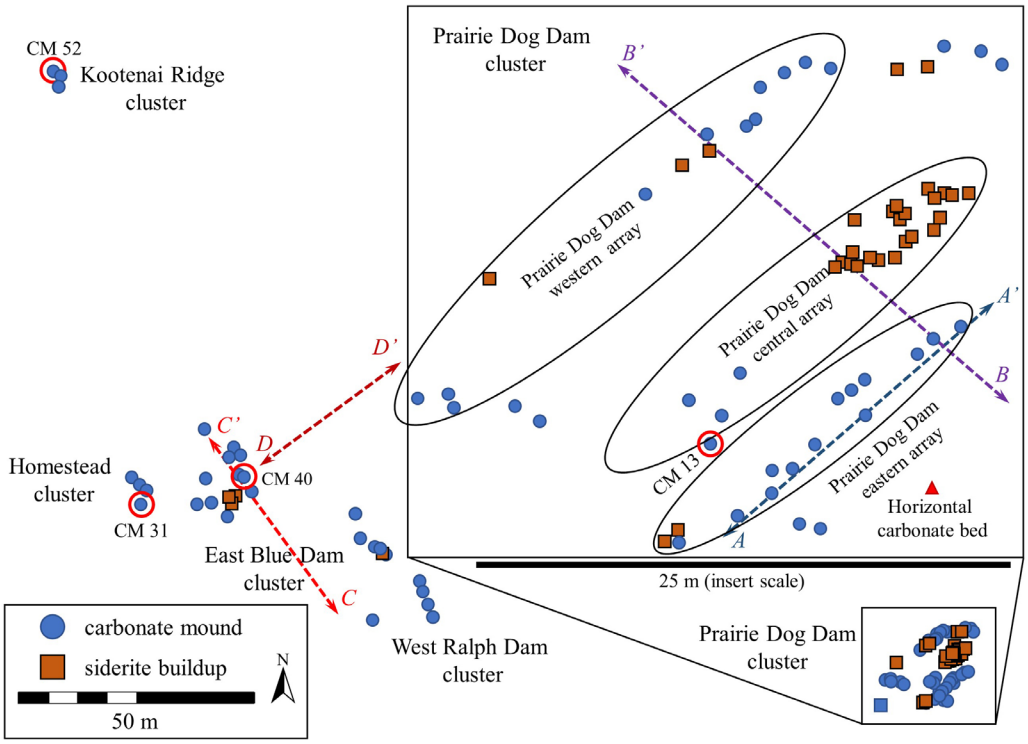

Figure 3. Spatial map of the carbonate and siderite buildups. The buildups are divided into clusters that are named based on local surface features. The Prairie Dog Dam cluster is subdivided into arrays (insert). The dashed lines A–A', B–B', C–C', and D–D' represent the electrical resistivity tomography (ERT) profiles herein described. The four carbonate mounds highlighted by the red circles are specifically referred to herein.

Description of Siderite Buildups

The Morrison Formation siderite buildups are typically found in clusters (e.g., Prairie Dog Dam cluster) but solitary siderite buildups are present (figure 3). The homogenous siderite buildups can be several meters in length but are less than half a meter in height (figure 4A). There are no sandstone beds, horizontal carbonate strata, or fossil fauna or flora associated with them. The buildups are more elongate than circular, and the uppermost surfaces are irregular from the protrusion of cone-in-cone apices (figures 4B and 4C). Cone-in-cone structures are common in the siderite buildups (figures 5A and 5B). In thin section, the siderite is homogenous displaying ghost traces of the cone-in-cone crystalline growth (figure 5C). Some carbonate mounds have siderite on the flanks and/or beneath an overlying mound (e.g., CM 40 and CM 52; figure 3). A large broad carbonate mound (CM 40) a meter in height with a 7-meter diameter overlays a siderite base (figure 6A). The carbonate-peripheral siderites also display small cone-in-cone structures (figure 5D).

XRD results on three siderite samples (SB 20, CM 40, 52) indicate the buildups are composed of 48.7% calcium carbonate ($CaCO_3$), 16.7% quartz (SiO_2), 16.0% siderite/ankerite ($CaFe(CO_3)/CaMgFe(CO_3)_2$), 10.5% illite, 7.3% kaolinite, and 0.9% pyrite (FeS_2).

XRF was performed on five different siderite buildups (SB 12, 18, 19, 32, 33; appendix) and two carbonate-peripheral siderites (SB 40.1, 40.2; figures 6A and 7). The three major elements for each siderite buildup are calcium (Ca), iron (Fe), and silica (Si). The analysis demonstrates a percentage variation in these three main elements as well as the trace elements (potassium [K], magnesium [Mg], titanium [Ti], manganese [Mn], alluminum [Al], phosphorus [P], sulfur [S], chlorine [Cl], and strontium [Sr]) (figure 7).

Standard isotope analysis was completed on two siderite buildups (SB 20, 40; table 1). The $\delta^{18}O$ siderite

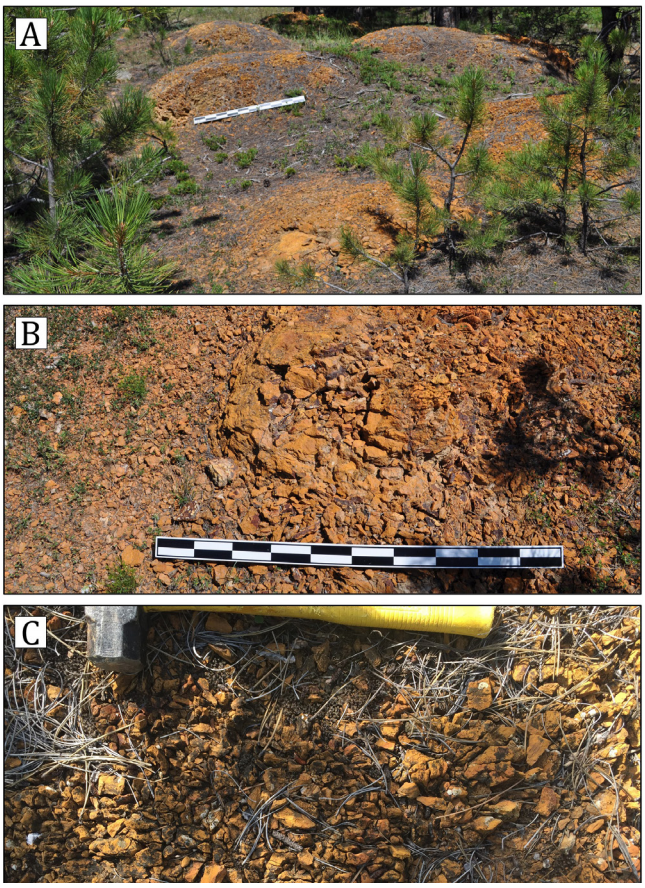

Figure 4. Field images of the siderite buildups. (A) Siderite buildups can be a few meters long but are less than 50 cm high. They can be isolated or found in clusters. (B and C) Closeup views of the siderite buildup's upper surfaces disrupted by cone-in-cone apices. Meter stick and hammer used for scale.

Table 1. Oxygen and carbon isotope data from carbonate buildups.

Sample	$\delta^{18}O$ ($^0/_{00}$ VPDB)	$\delta^{13}C$ ($^0/_{00}$ VPDB)
MT MRSN CM01	-12.03	-10.57
MT MRSN CM13	-16.72	-3.88
MT MRSN CM13*	-15.49	-4.32
MT MRSN CM14	-9.27	-4.88
MT MRSN CM17	-16.05	-6.78
MT MRSN CM27	-10.83	-5.04
MT MRSN CM31	-16.96	-5.83
MT MRSN CM35	-16.11	-4.53
MT MRSN CM35*	-16.00	-5.04
MT MRSN CM36	-12.85	-8.90
MT MRSN CM39	-15.48	-5.90
MT MRSN CM40	-15.48	-6.31
MT MRSN CM44	-11.83	-9.43
MT MRSN CM52	-15.59	-5.35
MT MRSN CM52*	-16.88	-6.50
MT MRSN CM62	-15.39	-6.25
MT MRSN CM66	-14.30	-5.46
MT MRSN SB20	-18.48	-5.49
MT MRSN SB40	-15.41	-5.08
NM TUFA SB1	-8.13	-6.40

CM — carbonate mound; SB — siderite buildup
*Different lab analyses

data have close values of -5.08‰ and -5.49‰ with a mean of -5.29‰. The $\delta^{13}C$ data ranges from -15.41‰ to -18.48‰ with a mean of -16.95‰.

Description of Carbonate Mounds

In contrast to the siderite buildups, the majority of the carbonate mounds are not found close to one another, but small clusters of carbonate mounds are present (figure 3). The homogenous carbonate mounds vary in length and height. The mounds are generally hemisphere-shaped, are typically a meter in diameter and less than a meter in height (figures 6B and 6C) although larger mounds are present. There are no sandstone beds or other terrestrial carbonate beds associated with the carbonate mounds. The mounds do not have macroscale cone-in-cone structures.

The majority of the carbonate mounds are composed of orthochemical micrite. Clastic detrital grains common in many terrestrial carbonates (e.g., travertines, tufas, calcretes, etc.) are absent. In general, allochems are rare. Few macrofossils are present with the carbonate mounds. Ten carbonate mounds have fossil wood in proximity to the mound but only three have fossil logs incorporated into the mound (CM 13, 31, 52). Typical macrophyte debris (leaves or twigs), hydrophytes, or charophytes are generally absent. Only two microscopic woody macrophyte fossil fragments were discovered. The first is unidentifiable woody debris (figure 8A); the second is a partial tangential fragment

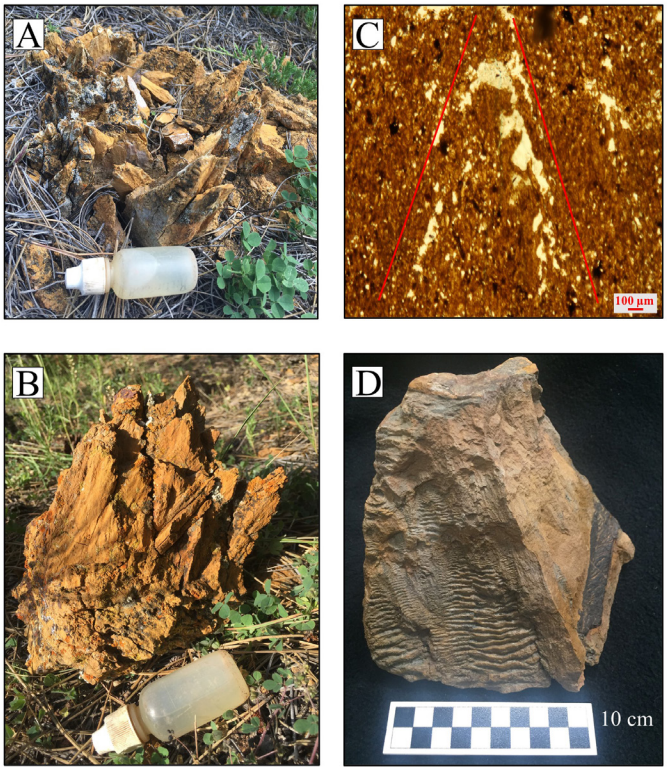

Figure 5. Images of cone-in-cone features of the siderite buildups. (A) Siderite cone-in-cone feature in place. (B) The same cone-in-cone feature is shown in A. This has been removed from the buildup to display the large size of the cone-in-cone feature. The 9-cm-long acid bottle is for scale. (C) Photomicrograph of a cone-in-cone feature from a siderite buildup. The cone-in-cone feature (red lines) is difficult to differentiate in the micritic matrix. (D) Along the flanks or underlying some carbonate mounds (e.g., CM 52) are pale yellowish-orange to dark yellowish-orange siderites. These are referred to as peripheral siderites and exhibit small cone-in-cone ridges. The sample shown is from beneath carbonate mound CM 52. The mound in shown in figure 6C.

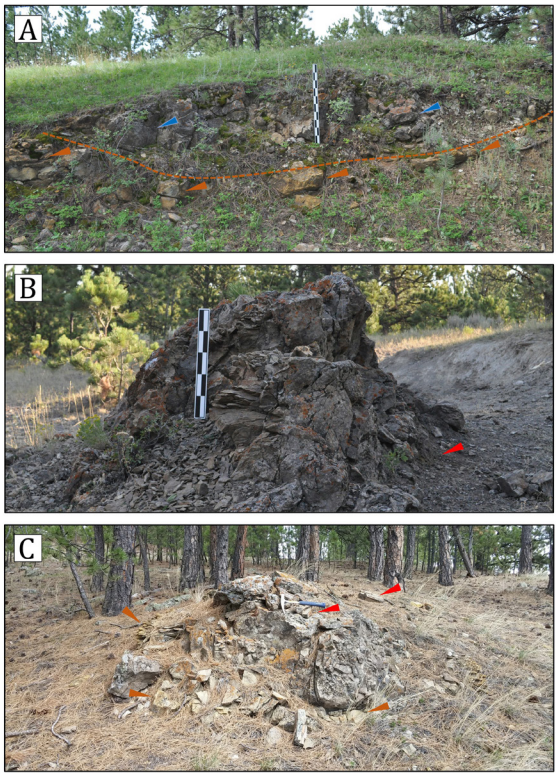

Figure 6. Field images of carbonate mounds. (A) Carbonate mound CM 40. The hemispherical shape of the carbonate mound is visible. The carbonate mound (blue arrows) also displays peripheral and underlying siderites (orange line and arrows). Meter scale. (B) Carbonate mound CM 13. The buildup had a partially encased fossil log of *Circoporoxylon* Kräusel. Unfortunately, the log was stolen. The red arrow shows where the log was present. In the background is the encasing illitic mudstone. 50 cm scale. (C) Carbonate mound CM 52. A fossil log of *Xenoxylon* Gothan is encased atop the mound (not visible). Some displaced fossil wood fragments are visible (red arrow). Peripheral siderites are visible at the base and sides of the carbonate mound (orange arrows). Hammer for scale.

of a homoxylous wood (figure 8B). In addition to the woody fragments, partial bryophyte leaves (liverworts; M. Philippe, University Lyon, written communication, 2020) are preserved in several mounds (CM 13, 17, 35; figure 8C). An organic fabric was discovered in mound CM 13 and might be tufa-associated green algae *Oocardium stratum* Nägeli (figure 8D). Fossil freshwater invertebrates such as ostracods or gastropods are not observed. Biogenic macrolaminae from cyanobacteria, typical of many terrestrial carbonates, are not observed. No trace fossils have been found.

Petrographic features of the carbonates include long dogtooth calcite crystals. Some dogtooth crystals appear to be coated with microbial films (figure 9A). Spherulites are observed in some carbonate mounds and have a very distinctive texture (figures 9B and 9C). Spherulites have a radiating array of crystalline fibers that developed from a nucleus (Beck and Andreassen,

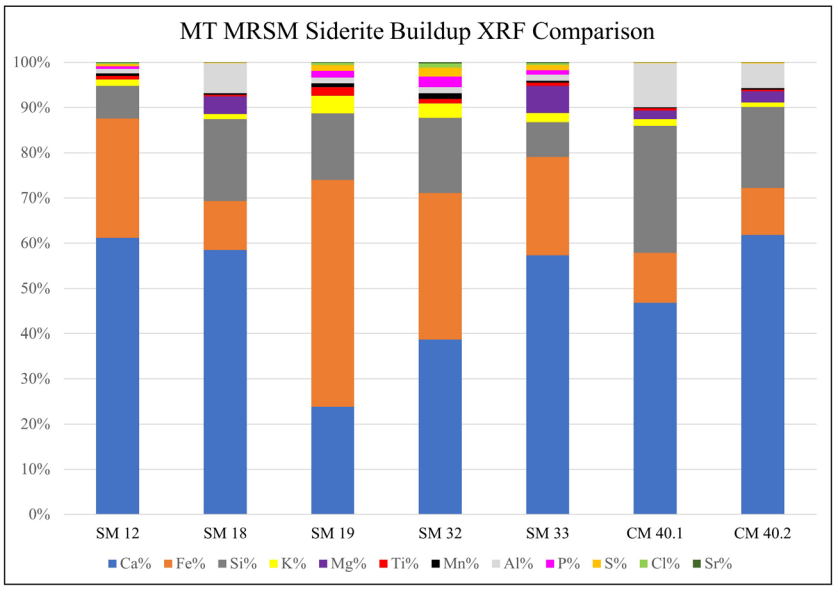

Figure 7. XRF comparison of several siderite buildups and two peripheral siderites (CM 40.1 and CM 40.2). The geochemical variability exhibited in the different buildups is thought to be the result of the interaction of the groundwater with different local soil chemistries during the development of the siderite buildup.

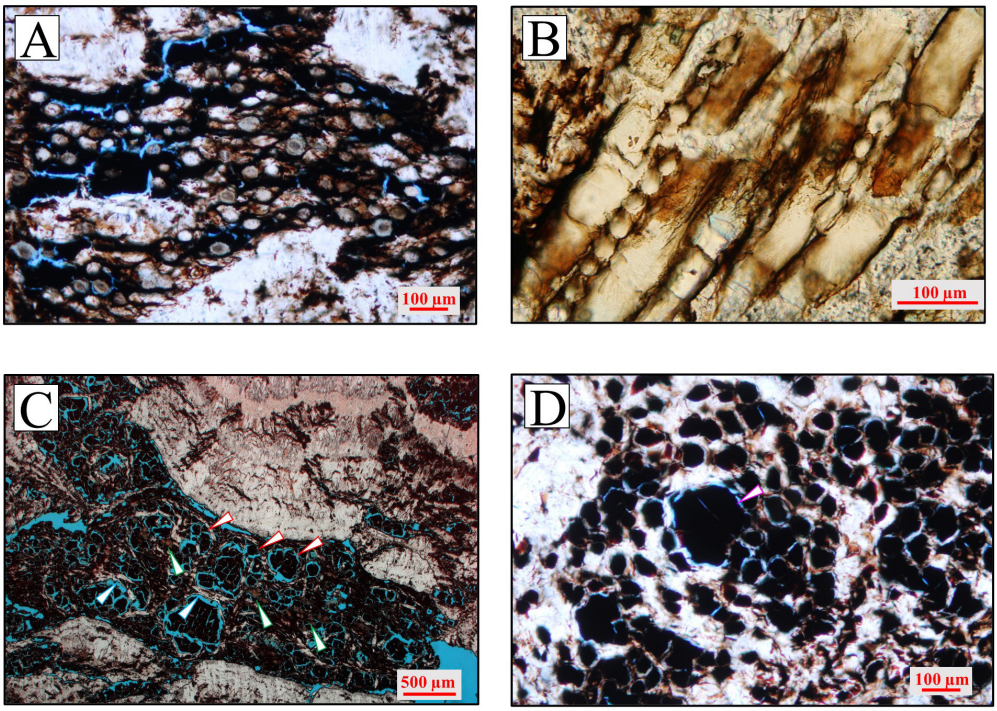

Figure 8. Photomicrographic images of fossil organic material found in some carbonate mounds. (A) Unknown fossil woody debris in thin section. (B) The tangential view of a fossil homoxylous woody plant. (C) A partial fossil bryophyte (liverwort) leaf. The circular chambers (red-outlined arrows) are filled with fossil cyanobacteria and bounded by the spongy mesophyll (blue-outlined arrows). Collenchymatous cells (cluster of brown cells) present in the midline of the leaf (green-outlined arrows) are common in extant liverworts. (D) The fossil circular pores resemble the features of *Oocardium stratum*, a green alga that is commonly associated with modern tufa deposits. The mean pore diameter is ≈ 30 µm. The large pore (pink-outlined arrow) may represent the stem of a fossil hydrophyte.

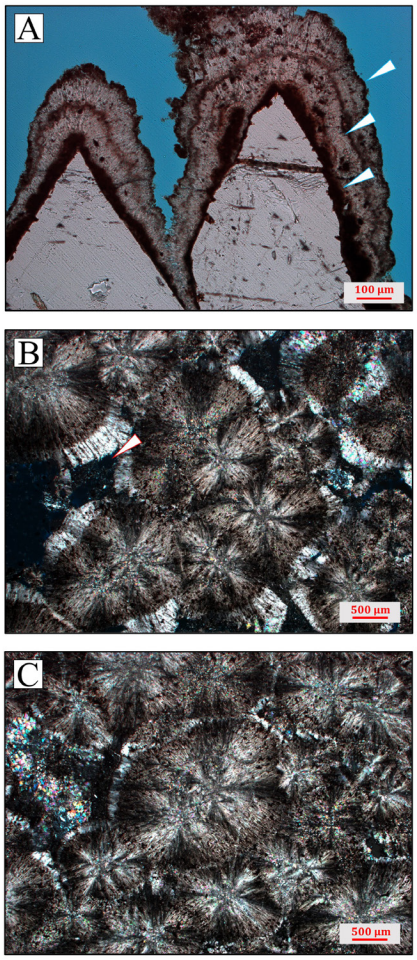

Figure 9. (A) Photomicrograph of dogtooth calcite crystals with cyanobacterial rinds (blue arrows) suggesting that crystals grew uninterrupted into a subaerial, carbonate-rich pool and the cyano-bacteria had access to sunlight. (B and C) Photomicrographs of spherulites. The spherulites are interpreted to be bacteria-derived. Refer to text for information on the bacteria. Primary porosity is evident (red arrow; dark blue epoxy). The dark spots scattered throughout the spherulites are fossil remnants of the bacteria. Images B and C are crossed nicols.

2010). Interestingly, the spherical crystal growth appears to have pushed organic material to the rim. Organic material is concentrated in the interstitial space between adjacent spherules. Occasionally organic material is encompassed by the spherule's mineral growth. The organic material is likely residual microphytes (algae) or bacteria (Chafetz and Folk, 1984). Many terrestrial carbonates have primary porosity. Primary porosity in the carbonate mounds is limited to intergranular spaces between the spherulites and the porous structures of macrophytes. In addition to the primary orthochemical micrite and radial-fibrous spherulites, many carbonate mounds have late diagenetic fractures annealed with sparry calcite.

XRD analysis was run on several carbonate mounds (CM 13, 38, 52, and 64). The data indicate that the carbonate mounds are composed of 98% calcium carbonate and 2% carbon. XRF was executed on eight different carbonate mounds. The three major elements are Ca, Fe in minor amounts, and Si. Variation in the three main elements and the trace elements (K, Mg, Ti, Mn, Al, P, S, Cl, and Sr) (figure 10) indicates that the geochemistry was distinct for each buildup. Two carbonate mounds (CM 13 and 52) were analyzed with XRF on a cm-scale cross section from the bottom of a large cut slab of the buildup moving upward (figures 11 and 12). Carbonate mounds 13 and 52 are stratigraphically separated by 5 m (figure 1). Both mounds incorporate fossil wood, *Circoporoxylon* Kräusel and *Xenoxylon* Gothan, respectively. The most noticeable variation for carbonate mound 13 is the percentage of Mg (figure 11; letters C, G, S, T). Carbonate mound 52 data displays more consistent chemistry with only minor differences (figure 12). The fossil wood (*Xenoxylon*; letters L-WD and M-WD) has distinct chemistry from the mound and implies wood preservation may involve nonmetals (Si, P, S, and Cl; figure 12).

Fourteen Morrison Formation carbonate mounds and a sample from the modern cascade tufa at Sitting Bull Falls, Sitting Bull Canyon, southwest of Carlsbad, New Mexico, were analyzed for standard isotope data (table 1). The $\delta^{18}O$ Morrison data displays variability ranging from -3.88‰ to -10.57‰ with a mean of -6.37‰. The $\delta^{13}C$ also shows variability ranging from -9.27‰ to -16.96‰ with a mean of -14.21‰. The mean $\delta^{13}C$ values are slightly lower than the pre-industrial revolution atmospheric value of meteoric water precipitated calcite (-6.5‰; NOAA data; Sharp, 2007).

Electrical Resistivity Tomography

Four localized electrical resistivity tomography (ERT) surveys were conducted to understand the

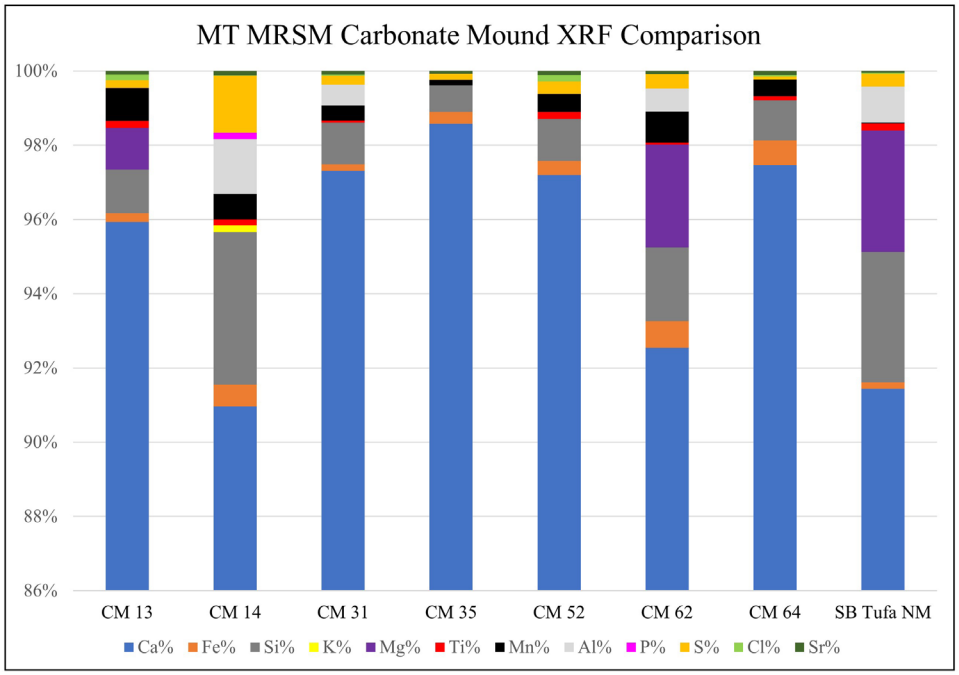

Figure 10. XRF comparison of several Morrison Formation carbonate mounds. The changes in mineralogical composition are likely a result of groundwater interaction with local strata and soils. The carbonate mound data represent different stratigraphic positions in the formation. No XRF measurements were made on fractures. The bar at the far right is data from the modern cascade tufa from Sitting Bull Falls, Sitting Bull Canyon, southwest of Carlsbad, New Mexico.

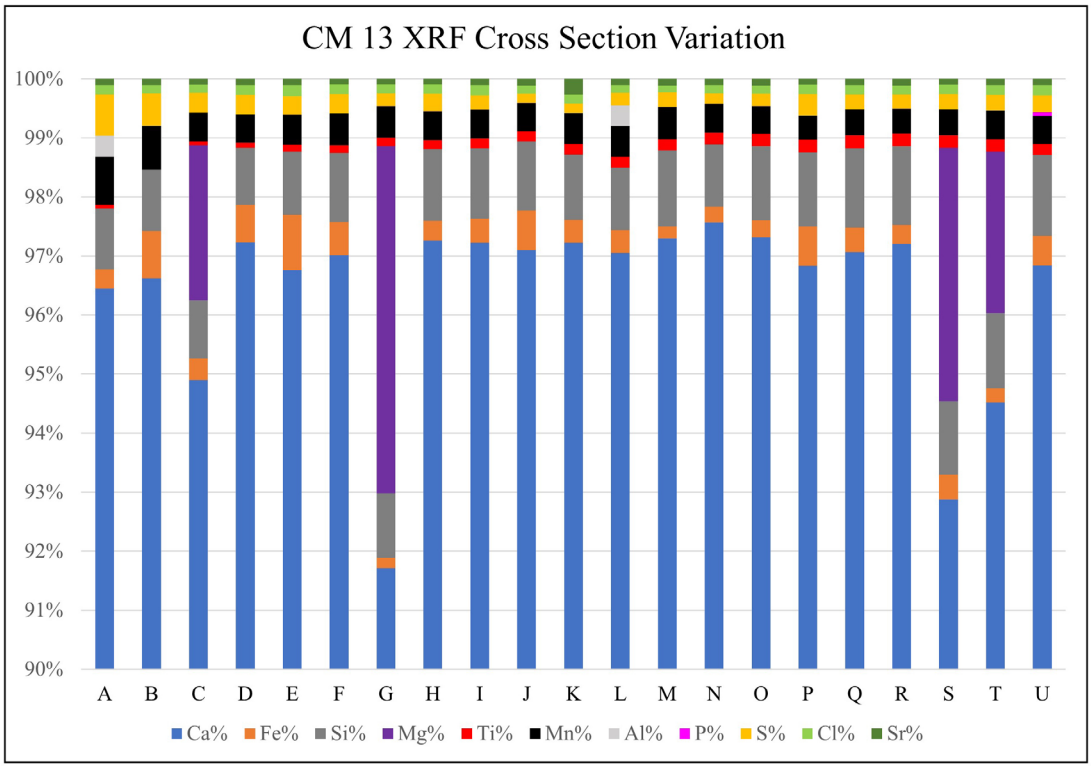

Figure 11. XRF data of CM 13 sampled at 1 cm increments. A large slab of the buildup was cut with measurement A at the bottom and moving upward. The most notable variation during the development of CM 13 is the increase in the percentage of magnesium (Mg). No XRF measurements were made on fractures.

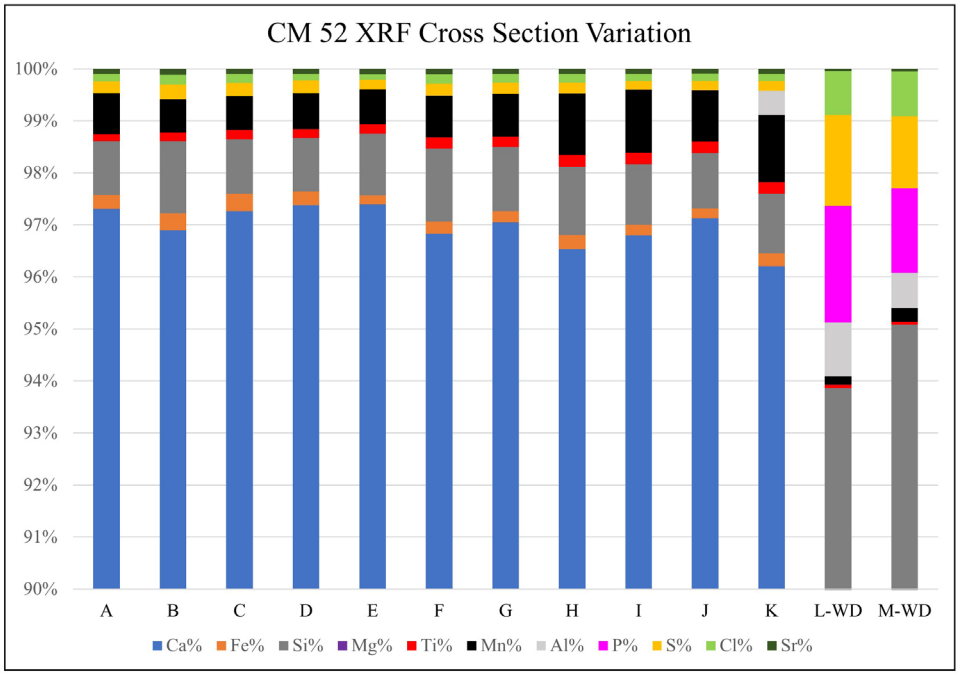

Figure 12. XRF data of CM 52 sampled at 1 cm increments. A large slab of the buildup was cut with measurement A at the bottom and moving upward. Sample CM 52 shows less variability in mineral percentages. Measurements L and M include fossil wood encased at the top of the carbonate mound. The unique chemical signature of the fossil wood implies preservation may involve Si, P, S, and Cl.

structure and potential subsurface continuation of the surface mounds, as was previously applied to delineate the subsurface continuation of a fossil tufa outcrop in northeast Spain (Huerta and others, 2016). On average, the obtained resistivities range from 20 to 200 Ω-m. Based on the correlation with outcrops and surface geology, two lithologies are interpreted to be present in the subsurface. Lithology 1 (carbonate) resistivities range from 150 to 200 Ω-m with thicknesses that range from 0.5 to at least 1.5 m. Lithology 2 (mudstone) resistivities range 10 to 70 Ω-m. The lowest resistivities associated with lithology 2 are attributed to the increased moisture content of some surface areas (dark blue) (figure 13).

ERT profile A–A' (figure 13A) was run parallel to the Prairie Dog Dam (PDD) eastern array (figure 3). Although we attempted to pass over several carbonate mounds, the ERT profile only shows high resistivity (> 150 Ω-m) at the distal ends of the profile. The northeastern buildup is about 6 m across. The profile does not show any additional high-resistivity carbonates (CM) in the subsurface.

ERT profile B–B' (figure 13B) was oriented perpendicular to profile A–A' trending northwest (figure 3) and crossing the western, central, and eastern PDD arrays. The surface high resistivity (> 150 Ω-m) at profile marker 58 m crosses over a small surface carbonate mound (figure 3). The ERT profile crosses many of the siderite buildups of the PDD central array between 86 to 100 m. This profile section displays low resistivities (< 25 Ω-m). Although the profile crosses over several surface siderite buildups, the buildups are not discernible in the profile. There are several potential reasons why the buildups are not seen in the profile. The topographic low where the siderite buildups reside may have had a higher water saturation (ephemeral creek bed). The buildups are highly fractured, and those fractures can hold conductive water. It is also possible that the siderite buildups are thin surface features that would make them indiscernible in the ERT since electrical current prefers conductive pathways. In

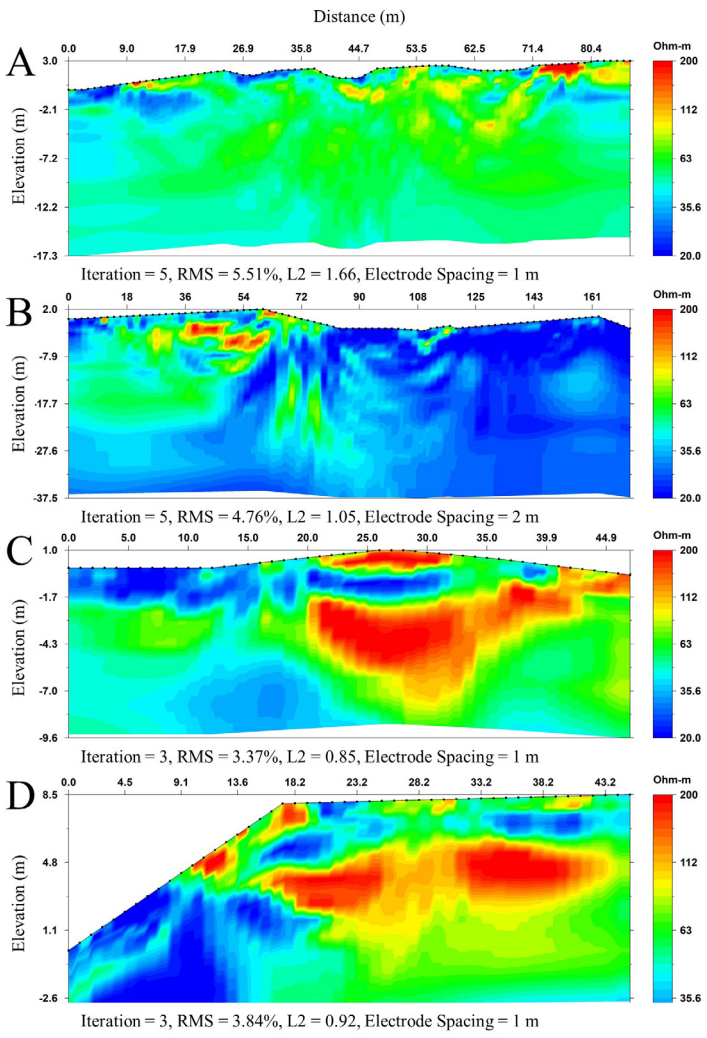

Figure 13. Electrical Resistivity Tomography (ERT) profiles (A to D). Refer to figure 3 for profile lines. (A) ERT Profile A–A' was run parallel to Prairie Dog Dam (PDD) eastern array. The ERT profile shows high resistivities (> 150 Ω-m) at the distal ends of the profile. The northeastern mound is about 6 m across. The profile does not show any additional high resistivity carbonates in the subsurface. (B) ERT profile B–B' at Prairie Dog Dam was oriented perpendicular to profile A–A' trending northwest across the western, central, and eastern arrays. The ERT profile crosses several siderite buildups of the PDD central array between 86 to 100 m. This profile section displays low resistivities (< 25 Ω-m) and the siderite buildups are not discernible in the profile. In contrast, the profile does differentiate a small carbonate mound from the PDD western array at 116 to 118 m. In the subsurface, between 36 to 60 m, is a high resistivity (110 to 200 Ω-m) zone, interpreted to be a large mound or possibly two mounds stratigraphically separated. (C) ERT profile C–C' was run parallel to the East Blue Dam cluster over the largest observed surface carbonate mound (CM 40). This mound is underlain by a thin siderite bed. The hemispherical mound is 7 m long and 1 m thick. Underlying the mound is a low resistivity zone (28 to 15 Ω-m) interpreted to be a ≈ 2-m-thick mudstone bed. Beneath this mudstone bed is a high resistivity zone (150 to 300 Ω-m) interpreted to be a significantly sized carbonate mound in the subsurface. The lateral extent of this mound may be as long as 15 to 41 m. The estimated minimum thickness is 1.5 m. Near the end of the profile, the high resistivities appear disjointed and stratigraphically higher and may represent another mound. (D) ERT profile D–D' was oriented perpendicular to profile C–C'. High resistivities (150 to 200 Ω-m) at profile marker 18.2 m represent a small surface buildup. Underlying the high resistivity zone is a lower resistivity zone (30 to 20 Ω-m). Similar to profile C–C', beneath the lower resistivity zone is a high resistivity zone (150 to 200 Ω-m). This zone is interpreted to represent a significantly sized buildup. The lateral extent of this mound is at least 24 m and may extend beyond the profile. The estimated thickness is 1 to 1.5 m. It should be noted that the large D–D' profile subsurface mound(s) has a different subsurface elevation than the large C–C' profile subsurface mound. Therefore, they are not stratigraphically equivalent.

contrast, the profile does discern a small carbonate mound from the PDD western array at 116 to 118 m. In the subsurface between 36 to 60 m is a high resistivity (110 to 200 Ω-m) zone interpreted to be a large mound or possibly two mounds separated stratigraphically.

ERT profile C–C' (figure 13C) was run parallel to the East Blue Dam cluster over the largest observed surface carbonate mound (CM 40; figure 3). The hemispherical mound (CM 40) is 7 m long and 1 m thick and is underlain by a thin siderite bed. Underlying the entire structure is a low resistivity zone (28 to 15 Ω-m) interpreted to be a ≈ 2-m-thick mudstone bed. Beneath this mudstone bed is a high resistivity zone (150 to 300 Ω-m) interpreted to be a significantly sized carbonate mound in the subsurface. The lateral extent of this mound may range from 15 to 41 m. The suggested minimum thickness is around 1.5 m

because ERT images tend to blur vertically with depth. Near the end of the profile, the carbonate subsurface layers appear disjointed and stratigraphically higher. This may be interpreted as representing a different smaller carbonate mound. Given the inherent low resolution of ERT imaging, however, this interpretation is speculative.

ERT profile D–D' (figure 13D) was oriented perpendicular to profile C–C' (figure 3). The high resistivities (150 to 200 Ω-m) at profile marker 18.2 m represent a small surface buildup. Underlying the high resistivity zone (CM) is a lower resistivity zone (30 to 20 Ω-m). Similar to profile C–C', below the lower resistivity zone is a subsurface high resistivity zone (150 to 200 Ω-m). This zone is interpreted to represent a significantly sized mound, or possibly two coeval mounds. The lateral extent of this mound is at least 24 m and may extend beyond the profile. The estimated thickness is 1 to 1.5 m. It should be noted the large D–D' profile subsurface mound(s) has a different subsurface elevation than the large C–C' profile subsurface mound. They are therefore not stratigraphically equivalent.

The four ERT surveys help to define the lateral extent of the surface mounds and the relative stratigraphy of several previously unknown carbonate mounds in the subsurface. The surface mounds and subsurface carbonates are decoupled by a thin low-resistivity zone that represents the encasing illitic mudstone. The ERT data indicate the presence of additional large stratigraphically isolated carbonate mounds in the subsurface.

Groundwater-fed Carbonate Deposits

Groundwater-fed carbonate deposits include travertine, tufas, sinters, and speleothems (Chafetz and Folk, 1984; Steinen, and others, 1987; Pedley, 1990; Golubic and others, 1993; Koban and Schweigert, 1993; Ford and Pedley, 1996; Pentecost and Coletta, 2007; Capezzuoli and others, 2014; Della Porta, 2015; Mohammadi and others, 2019). The classification of groundwater-fed carbonate deposits has a diverse history (see Jones and Renaut, 2010). Modern freshwater springs are categorized by the mean water temperature at the vent, where temperatures range from cold to boiling (Jones and Renaut, 2010). Pedley (1990) and Ford and Pedley (1996) use water temperature to delineate between travertine and tufa deposits. Herein we follow the general classification of Pedley (1990), but further define tufas as being precipitated under cooler water temperatures (< 20°C) whereas travertines as being precipitated under thermal conditions (> 20°C; Barilaro and others, 2012). Sinters can be siliceous or carbonaceous. They are commonly associated with hot springs or geysers in active volcanic terrains where mineral-charged geothermal fluids are discharged at the surface (Campbell and others, 2015; Munoz-Saez and others, 2016). At the other end of the temperature spectrum, speleothem deposits form in caves by evaporation of cool mineral-enriched waters.

Travertines are usually considered abiotic due to the hydrothermal water conditions that prohibit the existence of higher organisms (Chafetz and Folk, 1984; Koban and Schweigert, 1993; Ford and Pedley, 1996; Evans, 1999). Different invertebrates, plants, mosses, protozoa, algae, fungi, and bacteria have different tolerances of high-water temperature (Renaut and Jones, 2000). As discharged thermal waters flow away from the vent and cool, biota with differing temperature tolerances begin to inhabit these varying temperature zones. Travertine is enriched in ^{13}C and often contains high levels of sulfur (Pedley, 2009). Travertines tend to show less macrofacies diversity than tufa systems on account of their relatively limited lateral extent and biota (Ford and Pedley, 1996).

Cool water tufa carbonate precipitation occurs at ambient temperatures (< 20°C) and is usually associated with proximal paludal or lacustrine depositional facies (Pedley, 1990; Ford and Pedley, 1996). These tufas are characterized by the presence of heterotrophic bacteria, cyanobacteria, microphytes (algae), hydrophytes, macrophytes, and freshwater invertebrates (Kerney, 1959; Pedley, 1990; Ford and Pedley, 1996, Koban and Schweigert, 1993; Evans, 1999; Capezzuoli and others, 2014). Vertebrate fossils can also be associated with tufa deposits (Kerney, 1959; Springer and others, 2017). Inorganic precipitation (e.g., degassing CO_2) and organic microbial activity are important factors for carbonate precipitation in tufa environments. Tufa deposits have been further divided into allochthonous and autochthonous deposits (Pedley, 1990). Allochthonous tufas consist of either cemented

phytoclasts, intraclasts of silt- and sand-sized clasts sourced from tufas, micritic tufa material, or peloids and are usually associated with fluvial depositional systems (Pedley, 1990). Autochthonous tufas consist of stromatolitic horizontal laminations related to seasonal growth patterns of cyanobacteria (Janssen and others, 1999).

MORRISON FORMATION SIDERITE BUILDUPS AND CARBONATE MOUND SPRINGS

Interpretation of Near-surface Siderite Buildups

The Morrison siderite buildups are interpreted to be near-surface buildups and not surface tufa deposits. Siderite is the product of the interaction of numerous dynamic inorganic and organic systems. Groundwater chemistry is the summation of meteoric and subsurface water interactions with the local geology, aquifer lithologies, and soils. The availability and solubility of iron in soils are partly a byproduct of the decomposition of organic matter. Ferrous carbonate (siderite/ankerite) and ferric hydroxide (goethite and polymorphs) precipitate at a circumneutral pH (Hedrich and others, 2011). Acidic groundwater (pH < 4) causes iron and carbonate ($CaCO_3$) to remain in the solution. Alkaline groundwater (pH > 9) causes bicarbonate (HCO_3) to precipitate and release CO_2. To form siderite, the complexing agent $CaCO_3$ binds with the ferrous/ferric iron at a circumneutral pH (Blöthe and Roden, 2009). Soils in wet climates are typically acidic, whereas in dry climates the soils are alkaline (Slessarev and others, 2016). The interaction of acidic surface soil waters with alkaline groundwater likely developed the circumneutral pH required for proteobacteria to precipitate siderite.

In modern neutral pH freshwater environments iron-oxidizing phylum proteobacteria govern iron redox reactions (Blöthe and Roden, 2009; Hedrich, and others, 2011; Roden and others, 2012). Iron redox states are interconnected to inorganic compounds in soils and sediments. Micro-organisms play a fundamental function in iron redox reactions (Blöthe and Roden, 2009). Betaproteobacteria are the most common microbes in modern circumneutral pH freshwater environments including soil horizons (Roden and others, 2012). These lithotrophic iron-oxidizing bacteria often colonize in the soil transition zone between the anaerobic and aerobic subsurface environments (Roden and others, 2004). The position of the anaerobic/aerobic transition zone (i.e., the capillary fringe) can vary by precipitation, the upward migration of groundwater, or the deoxygenation of groundwater by microorganisms.

The Morrison Formation siderite buildups formed from precipitation-fed groundwater at the capillary fringe or by moving up small fractures as subsurface seeps into the vadose zone. The groundwater then interacted with the organic- and iron-rich forest soils and aided by iron-oxidizing betaproteobacteria resulting in siderite precipitation. The chemical variabilities of the siderite buildups as shown by the XRF data (figure 7) likely resulted from homogenous groundwater interacting with localized variable soil chemistries.

Cone-in-cone structures are common world-wide, known from every geologic age, and usually form in calcite, gypsum, or quartz (Cobbold and others, 2013). They commonly form in low-permeability saturated sediments such as shale or mudstone. Cobbold and others (2013) advocate that cone-in-cone structures develop from fractures that form coeval with mineral growth. The fractures are formed either by the force of crystallization, or fluid over-pressurization. Selles-Martinez (1994) agrees that crystalline fibers grow in saturated over-pressured regimes where fractures are induced by a decrease in pore pressure of the overlying sediments. In short, the difference between the saturated over-pressured zone (phreatic) and the hydrostatic zone (vadose) at the capillary fringe creates the boundary conditions that allow cone-in-cone structures to form. Although the paleoelevation of the capillary fringe is unknown, it is interpreted to have resided at a shallow burial depth based on the presence of peripheral-siderite buildups and owning to the similar elevation of proximal carbonate mounds.

Terrestrial siderites form in humid continental environments where precipitation exceeds evaporation. Siderites typically accumulate in poorly drained/anoxic wetland soils (Sheldon and Tabor, 2009; Ludvigson and others, 2013; Fernandez and others, 2014). The presence of the Morrison siderite buildups indicates a humid climate

with a near-surface groundwater capillary fringe. The siderite buildup cluster in the Prairie Dog Dam central array (figure 3) may be related to an anoxic wetland.

Interpretation of Carbonate Mound Springs

The carbonate mounds lack the many characteristics that are recognized to define modern groundwater-fed terrestrial deposits such as travertine and tufas. The Morrison carbonate mounds are composed of orthochemical micrite, show low primary porosity, display no cyanobacterial laminae, and fossil allochems are scarce. The general characteristics suggest the carbonate mounds may represent travertine deposits. However, as stated previously, there are no known Jurassic-aged hydrothermal sources to have created groundwater-fed carbonate mounds with water temperatures above 20° C. Carbon dioxide degassing is an important component of travertine deposition with the bubbles being preserved in the carbonate. These primary porosity structures are not observed in the field, nor in the thin sections for any of the studied Morrison carbonate mounds. This suggests CO_2 degassing was not violently occurring at the surface during precipitation and therefore the buildup was likely not hydrothermally sourced.

Fossil evidence and standard isotopic data indicate the carbonate mounds are tufa deposits. The incorporation of the microscopic woody macrophyte fossil fragments, homoxylous wood, bryophyte leaves (liverworts; figure 8), and the proximity of logs of *Cupressinoxylon*, *Circoporoxylon*, and *Xenoxylon* indicate that plants were growing near the mounds. Although different plants can have varying water temperature tolerances, the proximity to such a small diameter mound suggests an ambient water temperature. The fossilized microphyte fabric that may be the eukaryotic microalgae (Zygnematophyceae) *Oocardium stratum* Nägeli (Pfiester, 1976) also indicates water temperature. The calcifying desmid *O. stratum* is a colonial freshwater green alga commonly associated with modern tufas (Pentecost, 1991, 2005; Linhart and Schagerl, 2011). The pore diameter of the Morrison fossil microphyte is ≈ 30µ, whereas the pore diameter of the calcite tubes of modern *O. stratum* is between 17 to 20µ (Ibarra and Sanon, 2019). The alga *O. stratum* is known from waters with a temperature range from 7° to 13° C but can exist in cooler (4° C; Tran and others, 2019) or warmer water temperatures with an optimum water temperature of 13°C (Pentecost, 1991; Sanders and Rott, 2009; Linhart and Schagerl, 2011; Rott and others, 2012; Ibarra and others, 2014). Additional observed niche conditions for modern *O. stratum* include carbonate supersaturation, gradual CO_2 degassing, and circumneutral pH 7 to 8 in spring waters (Rott and others, 2012). Associated with the *O. stratum* are two 142µ diameter pores that may represent the stems of hydrophytes growing in association with the algae. If the fossil is *O. stratum*, its presence preserved in the carbonates indicates pH-neutral water with ambient temperatures (i.e., < 20° C).

Radial-fibrous spherulites are found in outcrop at the upper surfaces of the carbonate mounds. Spherulites are a common feature of fossil and modern tufa deposits (Guo and Chafetz, 2012) and are present in the modern Sitting Bull Falls tufa. Bacterially precipitated vaterite and calcite in marine and terrestrial environments are well documented (Boquet and others, 1973; Chafetz and Folk, 1984; Merz, 1992; Castanier and others, 2000; Braissant and others, 2003; Párraga and others, 2004; Ronholm and others, 2014; Baumann and others, 2016). Chafetz and Folk (1984) suggest bacterial carbonate precipitation may account for 90% of a tufa's framework grains. The spherulites are likely formed by the secretion of biofilms (i.e., glycocalyx) from betaproteobacteria such as *Ralstonia eutropha* H16 (Braissant and others, 2003), or a Jurassic variant. *R. eutropha* H16 is a chemolithoautotrophic bacterium able to grow within organic substrates under aerobic conditions (Müller and others, 2013). The modern bacterium *R. eutropha* H16 has an identical XRD diffractogram as calcium carbonate (Braissant and others, 2003). The bacterial formation of spherulites also indicates an ambient temperature.

The standard isotopic data of the carbonate mounds indicate that they are tufas. The $\delta^{18}O$ values are the product of meteoric water isotopic fractionation from latitude, elevation, precipitation and evaporation, seasonal temperature variation, and the precipitation of calcite (Dansgaard, 1964; Sharp, 2007). The mean $\delta^{18}O$ value derived from marine shell carbonates during the Late Jurassic (150 Ma) is –1‰ VPDB (Veizer and others, 1999).

In general, freshwater carbonates have negative $\delta^{13}C$ values, but these values can become even lighter if there are significant contributions of organic carbon (Sharp 2007). Paleo $\delta^{13}C$ values require a correction due to secular variation of the $\delta^{13}C$ throughout geologic time (Mackenzie and Pigott, 1981). The total dissolved carbon in the oceans has changed through geologic time. Variations in oceanic dissolved inorganic carbon are related to tectonism, erosion, productivity, and carbonate deposition (Sharp, 2007). During the Late Jurassic (150 Ma), the secular variation was near +2‰ VPDB (Veizer and others, 1999).

For terrestrial environments, the $\delta^{13}C$ of the freshwater carbonate is controlled by the dissolved inorganic carbon in the groundwater and its interaction with the soil. Carbonates precipitated at lower altitudes where vegetation productivity is generally higher (the Morrison planation surface of central Montana), should have lighter $\delta^{13}C$ values due to a greater contribution of ^{12}C from C_3 plants. At higher elevations, where plant productivity is poor, $\delta^{13}C$ will have isotopically heavier values.

Isotopic data of the Morrison tufa deposits (table 1) shows the $\delta^{18}O$ values are similar to the present weight annual $\delta^{18}O$ global distribution for comparable latitudes, suggesting minimal diagenetic alteration (Darling and others, 2006). Based on isotopic analysis of pedogenic carbonates and fossils, $\delta^{18}O$ values for paleometeoric waters of the Morrison Formation were highly depleted (Ekart and Cerling, 1996). The $\delta^{18}O$ values derived from fossil crocodile teeth and turtle scutes from four locations in the Morrison Formation show comparable values. From south to north the fossil localities are Kenton, OK; Fruita, CO; Nine Mile Hill, WY; and Upton, WY with the respective $\delta^{18}O$ values −16.14‰, −20.30‰, −16.31‰, and −16.94‰ (Brundridge, 2013). The central Montana $\delta^{18}O$ values (table 1) are slightly heavier than the more southern Morrison Formation $\delta^{18}O$ values signifying minor input from the retreating Sundance sea, perhaps due to changes in atmospheric circulation during the winter months.

The central Montana Morrison $\delta^{13}C$ data (table 1) indicate the dissolved inorganic carbon was derived from atmospheric CO_2 and the groundwater had a short residence time with minor interactions with organic matter in the soil (Darling and others, 2006; Sharp, 2007). Woody plants (C_3) are enriched in ^{12}C with values of $\delta^{13}C \approx -25‰$ (Park and Epstein, 1961; Sharp, 2007; Bacon and others, 2011) and the soils they produce have similar values (Diochon and Kellman, 2008). Pedogenic carbonates $\delta^{13}C$ values are dominated by the isotopic signal of plant communities (Sharp, 2007). The $\delta^{13}C$ values indicate these are not pedogenic carbonates.

The Morrison siderite buildup, carbonate mound, and the Sitting Bull Falls tufa standard isotopic data were plotted on a cartesian graph with $\delta^{18}O$ on the *x*-axis and $\delta^{13}C$ on the *y*-axis (figure 14). Fluvial and lacustrine tufas have negative $\delta^{18}O$ values. In contrast, lacustrine tufas have positive $\delta^{13}C$ values, whereas fluvial tufas have negative $\delta^{13}C$ values. In contrast, thermogenic waters exhibit low to very low negative $\delta^{18}O$ values coupled with positive $\delta^{13}C$ values. The negative $\delta^{18}O$ values indicate a meteoric source (Gandin and Capezzuoli, 2008; Della Porta, 2015), whereas the positive $\delta^{13}C$ values signify an increase in dissolved inorganic carbon as a result of deep subsurface circulation and longer residence times in limestone aquifers (Andrews, 2006).

The Sitting Bull Falls tufa plots as expected in the region for fluvial tufas. The Morrison siderite buildup and carbonate mound data consist of both negative $\delta^{18}O$ and $\delta^{13}C$ values. The Morrison isotopic data plots in the range of the oldest North American tufas, those associated with the Lower Jurassic Navajo Sandstone (Parrish and others, 2019). The negative isotopic values for the Morrison Formation siderite buildup and carbonate mound reveal that they were produced by meteoric waters in a continental setting (Andrews, 2006; Sharp, 2007). The isotopic data also provides insights into the variation of water chemistry during the mound formation. The main cluster of $\delta^{18}O$ values (mean −15.53‰) correspond to the expected values for the paleolatitude of $\approx 50^{o}$ north (Terzer, and others, 2013; Richmond and others, 2019a). In drier climates, the groundwater's residence time is increased owing to decreased recharge, resulting in isotopically heavier $\delta^{13}C$ values (Tanner, 2010). The negative $\delta^{13}C$ for the main cluster (mean −5.78‰) indicates the groundwater had a short residence time in the subsurface indicating regular and/or high precipitation.

Several isotopic data points diverge from the main

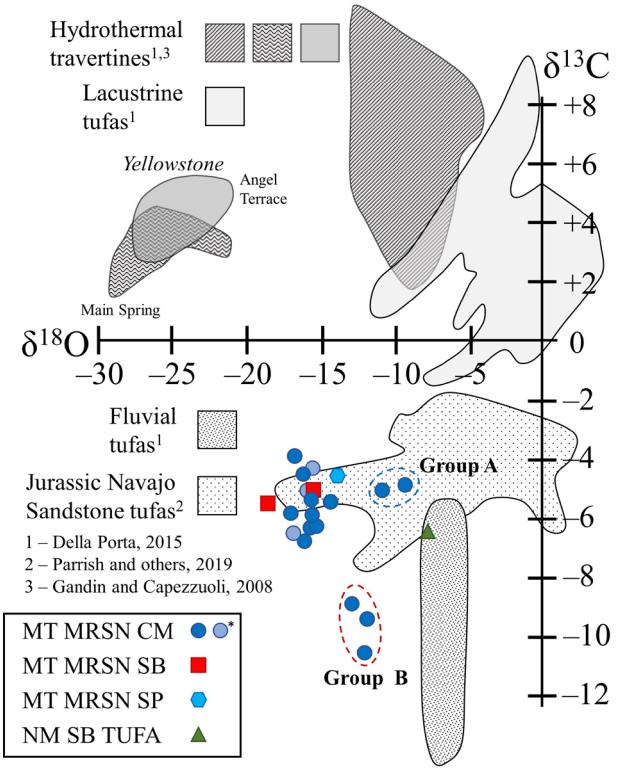

Figure 14. A plot of published standard isotopic data of tufas and travertines and the isotopic data from the central Montana Morrison Formation siderite buildups and mound springs. Plotted data indicates that the mound springs are freshwater tufa deposits. The dark blue circles represent carbonate mounds (CM), the red squares are siderite mounds (SB), the light blue circles are carbonate mounds run at another lab for comparison. The green triangle represents the modern cascade tufa at Sitting Bull Falls, Sitting Bull Canyon, southwest of Carlsbad, New Mexico. The isotopic data shows that the buildups are ambient water-temperature tufa mounds. These are the first tufa mounds recorded for the Morrison Formation and are the second oldest tufa deposits in North America. The isotopic data also provides some insights into the variation in water chemistry. The $\delta^{18}O$ matches the expected paleolatitude of the region. A few data points show variance in the geochemistry recorded by the tufas. The $\delta^{13}C$ for the central cluster indicates the groundwater had a low residence time in the subsurface indicating regular and/or high precipitation. The more negative $\delta^{18}O$ values in Group A suggest there may have been precipitation input from northern storms from the retreating Sundance sea. The more negative $\delta^{13}C$ values of Group B suggest drier periods resulting in a longer subsurface residence time allowing groundwater to interact with plant carbon in the subsurface.

data cluster, but these present insights into the climatic variance recorded by the tufas. The less negative $\delta^{18}O$ values (figure 14, Group A; mean -10.05‰) implies a marine isotopic component. Changes in atmospheric circulation may have brought northern-sourced precipitation from the Sundance sea to central Montana. The more negative $\delta^{13}C$ values (figure 14, Group B; mean -8.31‰) indicate short drier periods resulted in a longer subsurface residence time allowing groundwater to interact with plant carbon in the subsurface. The difference between the positive Late Jurassic oceanic $\delta^{13}C$ values (+2‰) and the negative values (mean -6.13‰) of the Morrison Formation of central Montana suggest the region had a low elevation with high plant productivity and a wet climate.

The observed and inferred characteristics of the Morrison carbonate tufa mounds are analogous with the artesian mound springs of the Great Artesian Basin (GAB) in the Lake Eyre South region of southern Australia (Keppel and others, 2011, 2012). The GAB mound springs acquired their name for their hemispherical shape that forms by the accretion of sediment around the spring

outlet. The outlet gradually rises in elevation forming a dome- or shield-shaped cone and are typically between 2 to 5 m in height (Williams and Holmes, 1978; Keppel and others, 2011). Many GAB mound springs do not consist of the characteristic calcareous mound but either emerges at ground level or consist of soft, silty mounds. The GAB mound springs form under a semiarid to arid climate (Harris, 1981). The GAB-associated paludal environments are limited in size due to the high rates of evaporation (> 10 mm/day; Holmes and others, 1981). GAB mound spring formation is related directly to a low flow rate (Ponder, 1986). Springs with higher flow rates have associated channels (i.e., spring tails) that distribute the discharged fluids away from the spring vent, whereas decreased flow rates allow for the precipitation at the vent, resulting in the building up of the mound. The GAB mound springs are composed of eolian sand, plant debris, and mud and sand carried up through fractures by the spring discharge (Ponder, 1986). According to Stokes law, a discharge rate of greater than 4 cm/s is required to lift fine sand within a fracture (Williams and Holmes, 1978).

The Morrison carbonate mound springs are similar in shape to the GAB mound springs but have a subartesian component. No detrital sand or clay has been found in the Morrison mound springs suggesting discharge rates were < 4 cm/s. Low flow rates facilitated the building of the mound. The lack of associated fluvial, paludal, or lacustrine facies supports the interpreted low surface discharge rate. The spatial distribution of the siderite buildups and carbonate mounds in proximity to Late Jurassic faults or fractures corresponds to the azimuth orientation of the present-day major Montana lineaments (figure 15).

The Morrison floral productivity in central Montana is a manifestation of low elevation and precipitation rates. The floral productivity resulted in abundant decomposing organic carbon on the forest floor and into the shallow subsurface. The precipitation and groundwater geochemically interacted with the organic carbon to produce more negative $\delta^{13}C$ values. The high productivity of the region (Rees and others, 2000, 2004), and the low negative $\delta^{13}C$ values suggest that the groundwater had a relatively short residence time in the subsurface otherwise the $\delta^{13}C$ values would have been substantially isotopically lighter (≈ −25‰). In contrast, a relatively longer subsurface residence time is suggested by the isotopic values for Group B in figure 14.

Paleoclimatic Significance

Morrison Formation sediments are interpreted to have been deposited under a strongly seasonal arid to semi-arid climate (Dodson and others, 1980; Parrish and others, 1982, 2004; Hotton, 1986; Parrish and Peterson, 1988; Turner and Fishman, 1991; Valdes and Sellwood, 1992; Demko and Parrish, 1998; Demko and others, 2004). The aridity was likely generated by several factors including the latitudinal position in the subtropical dry belt, the Sevier orogenic belt acting as a rain shadow (Demko and Parrish, 1998), and oceanic upwelling driven by coastal wind patterns (Parrish and Peterson, 1988). Peterson and Turner-Peterson (1987) suggested the presence of narrow but extensive riparian environments that supported abundant plant life to sustain the large herbivorous dinosaurs that roamed the Morrison basin.

Similar to modern continentality, the proximity of the northward-retreating Sundance sea during the Late Jurassic likely created cool and wet coastal climates in central Montana in contrast to the more southern inland continental regions. Palynological research over the Morrison basin shows the paleoclimate transitioned from arid in the southern latitudes to a more humid climate in the northern clines (Hotton and Baghai-Riding, 2010; Baghai-Riding and others, 2015). The discovery of the boreal wood *Xenoxylon* in the Morrison Formation of central Montana corroborates a wet climate in the northern basin latitudes (Richmond and others, 2019a). The newly discovered partial bryophyte leaves with their chambers occupied by cyanobacteria also provide some insights into the paleoclimate. Bryophytes live in a wide variety of habitats; however, they prefer moist environments (Schuster, 1966; Shaw and Renzaglia, 2004). Their preservation in mound springs indicates proximity to the outlet. If the microphyte fabric is *O. stratum* or a close relative, then its presence in association with the Morrison carbonate mound springs provides additional insights into the paleoclimate of the Morrison Formation of central Montana. Modern

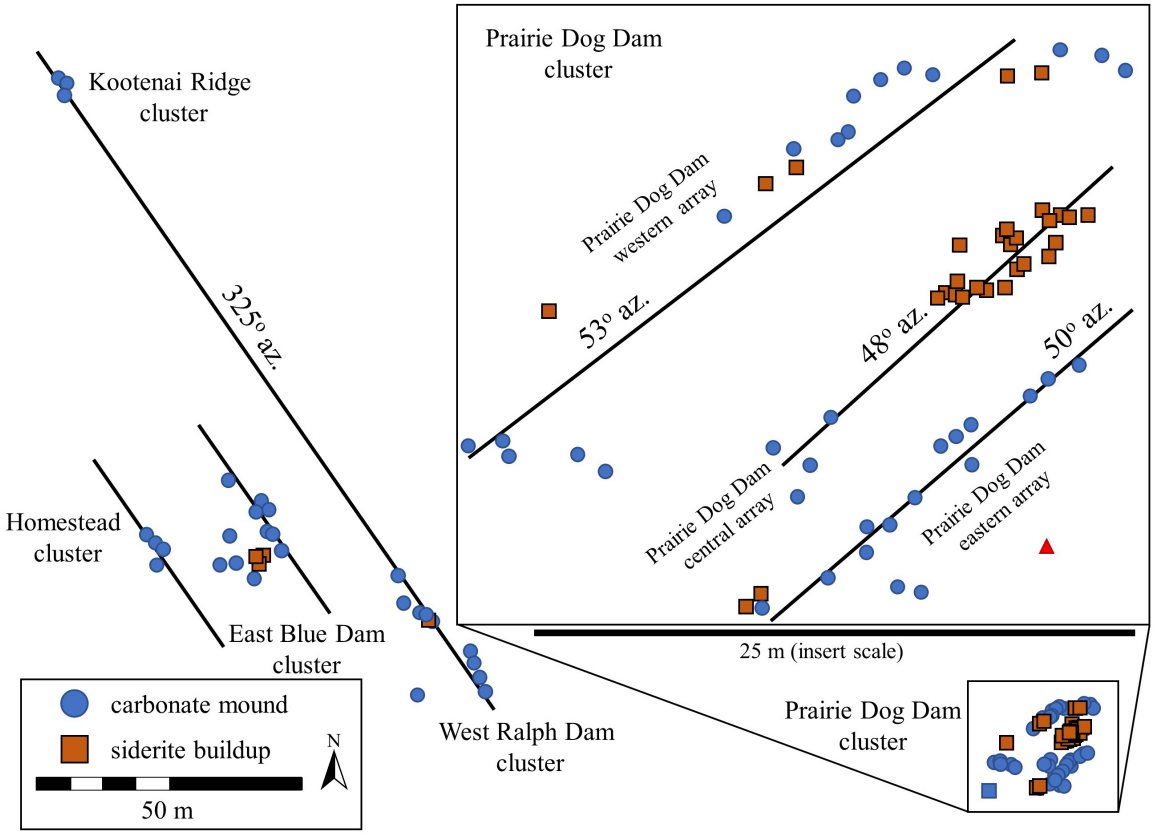

Figure 15. Spatial map of the carbonate and siderite buildups. The buildups are divided into clusters. The insert shows the Prairie Dog Dam cluster arrays. Lines of best fit for the respective arrays and clusters are shown. The azimuth bearing of each line is similar to the strike of the regional lineaments of Montana, suggesting a correlation between the buildups and the structural lineaments. Refer to figure 2 for the locations of the structural lineaments.

O. stratum is present in warm- and cool-temperate climates (Pentecost, 1990, 2005) but is more prevalent in regions where summer temperatures exceed 25°C (Pentecost, 1991).

Semi-arid conditions are incapable of sustaining the perennial highwater table necessary for continuous discharge to form tufa deposits (Pedley, 1990). Consequently, regions with higher rainfall and temperatures promote tufa formation (Ford and Pedley, 1996). An average annual temperature between 5° to 15° C is suggested to be the most favorable to tufa formation and growth (Pentecost, 1991; Ibarra and others, 2014).

Stable isotope data from the mound springs have a negative $\delta^{18}O$. This verifies that during the Late Jurassic central Montana's paleolatitude was between 40° to 50° (Richmond and others, 2019a) and that the area experienced increased rainfall. Tufas generally occur in regions characterized by an annual rainfall over 500 mm/year (Pentecost, 1991; Ibarra and others, 2014). Tufas with *Oocardium* commonly have rainfall that exceeds 1000 mm/year (Ibarra and others, 2014). Using the elemental analyses to calculate the calcium and magnesium weathering index (CALMAG) of paleosol B horizons in the Morrison Formation of south-central Montana, Myers and others (2014) estimated a mean annual rainfall for the region ≈ > 1200 mm/year. The occurrence of the tufas and a varied paleoflora and the CALMAG data of Myers and others (2014) indicate that during the Late Jurassic central Montana experienced a warm temperate (Rees and others, 2004) to cool temperate climate with dry warm summers and with increased precipitation during the cool winter months.

The ERT data displays the presence of larger mounds in the subsurface, with mudstone strata between the

surface and the subsurface mounds. These subsurface data provide two inferences about the mounds. First, the larger mounds record a prolonged period of increased precipitation. Second, the environmental conditions required for the mounds were not continuous. The separation of the subsurface and surface by mudstone deposition suggests that there were dry periods with insufficient precipitation to create mounds. The numerous carbonate mound springs, and their variable stratigraphic positions within the formation (40 to 52 m), suggest wet cycles during the Late Jurassic of central Montana, interspersed with drier periods of undetermined duration.

CONCLUSIONS

The discovery of numerous mound springs represents the first observed occurrence of tufa deposits in the Morrison Formation and some of the oldest tufa deposits documented for North America (Dorney and others, 2017; Parrish and others, 2017, 2019). The spatial data demonstrate a linear relationship to the buildups and mounds that were likely sourced by carbonate-rich water from fractures along Jurassic-aged lineaments. The siderite buildups, with their cone-in-cone structures, formed in the subsurface near the capillary fringe. In the subsurface, the groundwater interacted with the iron-rich soils of the forest floor. XRF data of the various siderite buildups suggest a variable chemistry caused by the groundwater interacting with local soils. Betaproteobacteria advanced the precipitation of the iron carbonates in the subsurface. The carbonate mound springs formed from groundwater surface seeps leaking up fractures. Spring flow rates are interpreted to have been subartesian, as there are no connecting fluvial or lacustrine facies. The precipitation of the carbonate mounds was inorganic and organic. The presence of spherulites shows that betaproteobacteria played a part in the carbonate precipitation. The mound spring waters discharged at the surface are interpreted to have been cool (< 20°C) based on the isotopic data, the lack of evidence for CO_2 degassing at the vent, low sulfur percentages, and the associated algal material (e.g., *Oocardium*). The presence of the algal material in the spherulites, algal films on the dogtooth calcite crystals, the incorporation of *Oocardium*, bryophyte leaves, and homoxylous wood of gymnosperm logs into the mounds also indicate the mounds formed at the surface with plants living near the springs.

The isotopic $\delta^{13}C$ data indicate that the groundwater was meteoric in origin, occurring in a low elevation continental setting that experienced high rainfall. The stratigraphic sections and the ERT subsurface data of the mound springs imply repeated periods of increased precipitation separated by drier periods. This wet climate for the Morrison Formation of central Montana is in contrast to the climate models and interpretations of the more southern regions.

ACKNOWLEDGMENTS

We especially thank the Hein family for access to their ranch and their wonderful support during this research project. The senior author is grateful to Nate Murphy of Judith River Dinosaur Institute, Billings Montana, for his continuous field support and use of field equipment. The senior author also wishes to express appreciation to Dr. Judith Totman Parrish (University of Idaho, emerita) and Dr. Giovanna Della Porta (University of Milan) for insights and discussions.

REFERENCES

Andrews, J.E., 2006, Palaeoclimatic records from stable isotopes in riverine tufas—synthesis and review: Earth-Science Reviews, v. 75, p. 85–104.

Bacon, K.L., Belcher, C.M., Hesselbo, S.P., and McElwain, J.C., 2011, The Triassic–Jurassic boundary carbon isotope excursions expressed in taxonomically identified leaf cuticles: Palaios, v. 26, p. 461–469.

Baghai-Riding, N., Hotton, C.L., Davis, K., and Davidson, T., 2015, Palynological evidence for a latitudinal moisture gradient in the Late Jurassic Morrison Formation [abs.]: Geological Society of America Abstracts with Programs, v. 47, no. 7, p. 143.

Barilaro, F., Della Porta, G., and Capezzuoli, E., 2012, Depositional geometry and fabric types of hydrothermal travertine deposits (Albegna Valley, Tuscany, Italy): Rendiconti online della Società Geologica Italiana, v. 21, p. 1024–1025.

Baumann, L.M.F., Birgel, D., Wagreich, M., and Peckmann, J., 2016, Microbially-driven formation of Cenozoic siderite and calcite concretions from eastern Austria: Austrian Journal of Earth Sciences, v. 109, p. 211–232.

Beck, R., and Andreassen, J.-P., 2010, Spherulitic growth of calcium carbonate: American Chemical Society Crystal Growth and Design, v. 10, p. 2934–2947.

Blöthe, M., and Roden, E. E., 2009, Microbial iron redox cycling in a circumneutral-pH groundwater seep: Applied and Environmental Microbiology, v. 75, p. 468–473.

Boquet, E., Boronat, A., and Ramos-Cormenzana, A., 1973, Production of calcite (calcium carbonate) crystals by soil bacteria is a general phenomenon: Nature, v. 246, p. 527–528.

Braissant, O., Cailleau, G., Dupraz, C., and Verrecchia, E. P., 2003, Bacterially induced mineralization of calcium calcite in terrestrial environments—the role of exopolysaccharides and amino acids: Journal of Sedimentary Research, v. 73, p. 485–490.

Brown, R.W., 1946, Fossil plants and Jurassic-Cretaceous boundary in Montana and Alberta: American Association of Petroleum Geologists Bulletin, v. 30, p. 238–248.

Brundridge, K., 2013, Assessing latitudinal variations in climate of the Jurassic Morrison Formation from oxygen isotopes from aquatic vertebrates: San Antonio, University of Texas at San Antonio, M.S, thesis, 65 p.

Campbell, K.A., Guido, D. M., Gautret, P., Foucher, F., Ramboz, C., and Westall, F., 2015, Geyserite in hot-spring siliceous sinter—window on Earth's hottest terrestrial (paleo)environment and its extreme life: Earth-Science Reviews, v. 148, p. 44–64.

Capezzuoli, E., Gandin, A., and Pedley, M., 2014, Decoding tufa and travertine (fresh water carbonates) in the sedimentary record—the state of the art: Sedimentology, v. 61, p. 1–21.

Castanier, S., Le Métayer-Levrel, G., and Perthuisot, J.-P., 2000, Bacterial roles in the precipitation of carbonate minerals, *in* Riding R.E., and Awramik S.M., editors, Microbial Sediments: Berlin, Springer-Verlag, p. 32–39.

Chafetz, H.S., and Folk, R. L., 1984, Travertines—depositional morphology and the bacterially constructed constituents: Journal of Sedimentary Petrology, v. 54, p. 289-316.

Cobbold, P.R., Zanella, A., Rodrigues, N., and Løseth, H., 2013, Bedding-parallel fibrous veins (beef and cone-in-cone)—worldwide occurrence and possible significance in terms of fluid overpressure, hydrocarbon generation and mineralization: Marine and Petroleum Geology, v. 43, p. 1–20.

Darling, G.W., Bath, A.H., Gibson, J.J., and Rozanski, K., 2006, Isotopes in water, *in* Leng, M.J., editor, Isotopes in palaeoenvironmental research: Developments in Paleoenvironmental Research, v. 10, p. 1–66.

Dansgaard, W., 1964, Stable isotopes in precipitation: Tellus, v. 16, p. 437–468.

Della Porta, G., 2015, Carbonate build-ups in lacustrine, hydrothermal, and fluvial settings: comparing depositional geometry, fabric types and geochemical signature, *in* Bosence, D.W.J., Gibbons, K.A., Le Heron, D.P., Morgan, W.A., Pritchard, T., and Vining, B.A., editors, Microbial carbonates in space and time—implications for global exploration and production: Geological Society of London Special Publication 418, p. 17–68.

Demko, T.M., Currie, B.S., and Nicoll, K.A., 2004, Regional paleoclimatic and stratigraphic implications of paleosols and fluvial/overbank architecture in the Morrison Formation (Upper Jurassic), Western Interior, USA: Sedimentary Geology, v. 167, p. 115–135.

Demko, T.M., and Parrish, J.T., 1998, Paleoclimatic setting of the Upper Jurassic Morrison Formation: Modern Geology, v. 22, p. 283–296.

Diochon, A., and Kellman, L., 2008, Natural abundance measurements of ^{13}C indicate increased deep soil carbon mineralization after forest disturbance: Geophysical Research Letters, v. 35, L14402, p. 1–5.

Dodson, P., Behrensmeyer, A.K., Bakker, R.T., and McIntosh, J.S., 1980, Taphonomy and paleoecology of the dinosaur beds of the Jurassic Morrison Formation: Paleobiology, v. 6, p. 208–232.

Dorney, L.J., Parrish, J.T., Chan, M.A., and Hasiotis, S.T., 2017, Petrography and environmental interpretation of tufa mounds and carbonate beds in the Jurassic Navajo Sandstone of southeastern Utah, U.S.A.: Journal of Sedimentary Research, v. 87, p. 967–985.

Dupree, R.T., 2009, Provenance of Lower Kootenai (Lower Cretaceous) fluvial sandstone bodies, Sandy Hollow/Big Hole River area, southwestern Montana: Lafayette, University of Louisiana at Lafayette, M.S. thesis, 84 p.

Ekart, D.D., and Cerling, T.E., 1996, pCO_2 during deposition of the Late Jurassic Morrison Formation and other paleoclimatic/ecologic data as inferred by stable carbon and oxygen isotope analyses [abs.]: Geological Society of America, Abstracts with Programs, v. 28, no. 7, p. 252.

Evans, J.E., 1999, Recognition and implications of Eocene tufas and travertines in the Chadron Formation, White River Group, Badlands of South Dakota: Sedimentology, v. 46, p. 771–789.

Everett, M.E., 2013, Near-surface applied geophysics: Cambridge University Press, 403 p.

Fernandez, A., Tang, J., and Rosenheim, B.E., 2014, Siderite 'clumped' isotope thermometry—a new paleoclimate proxy for humid continental environments: Geochimica et Cosmochimica Acta, v. 126, p. 411–421.

Ford, T.D., and Pedley, H.M., 1996, A review of tufa and travertine deposits of the world: Earth-Science Reviews, v. 41, p. 117–175.

Foster, J., 2007, Jurassic West—the dinosaurs of the Morrison Formation and their world: Bloomington, Indiana University Press, 389 p.

Fuentes, F., DeCelles, P.G., Constenius, K.N., and Gehrels, G.E., 2011, Evolution of the Cordilleran foreland basin system in northwestern Montana, U.S.A.: Geological Society of America Bulletin, v. 123, p. 507–533.

Gandin, A., and Capezzuoli, E., 2008, Travertine versus calcareous tufa—distinctive petrologic features and stable isotope signatures: Italian Journal of Quaternary Sciences, v. 21, p. 125–136.

Gardner, L.S., 1950, Geology of the Button Butte-Forestgrove area, Fergus County, Montana: U.S. Geological Survey Oil and Gas Investigations Preliminary Map OM-106, 1 plate, scale 1:63,360.

Golubic, S., Violante, C., Ferreri, V., and D'Argenio, B., 1993, Algal control and early diagenesis in Quaternary travertine formation (Rocchetta a Volturno, central Apennines): Bollettino della Societa Paleontologica Italiana, v. 1, p. 231–247.

Guo, X., and Chafetz, H.S., 2012, Large tufa mounds, Searles Lake, California: Sedimentology, v. 59, p. 1509–1535.

Harris, C., 1981, Oases in the desert—the mound springs of northern South Australia: Proceedings of the Royal Geographical Society of Australasia, South Australian Branch, v. 81, p. 26–39.

Harris, W.L., 1966, The stratigraphy of the Upper Jurassic-Lower Cretaceous rocks in the Great Falls-Lewistown coal field, central Montana, *in* Cox, J.E., editor, Jurassic and Cretaceous stratigraphic traps, Sweetgrass arch: Billings Geological Society 17th Annual Field Conference, p. 164–177.

Hedrich, S., Schlömann, M., and Johnson, D.B., 2011, The iron-oxidizing proteobacteria: Microbiology, v. 157, p. 1551–1564.

Holmes, J.W., Williams, A.F., Hall, J.W., and Henschke, C.J., 1981, Measurements of discharges from some of the mound springs in the desert of northern south Australia: Journal of Hydrology, v. 49, p. 329–339.

Hotton, C.L., 1986, Palynology of the Morrison Formation [abs.]: Proceedings of the Fourth North American Paleontological Convention, p. A20.

Hotton, C., and Baghai-Riding, N., 2010, Palynological evidence for conifer dominance within a heterogeneous landscape in the Late Jurassic Morrison Formation, U.S.A., *in* Gee, C., editor, Plants in Mesozoic time: Bloomington, Indiana University Press, p. 295–328.

Huerta, P., Armenteros, I., Tomé, O.M., Gonzálvez, P.R., Silva, P.G., González-Aguilera, D., and Pedro Carrasco-García, P., 2016, 3-D modelling of a fossil tufa outcrop—the example of La Peña del Manto (Soria, Spain): Sedimentary Geology, v. 333, p. 130–146.

Hutsinpiller, A., and Parry, W.T., 1985, Geochemistry and geothermometry of spring water from the Blackfoot reservoir region, southwestern Idaho: Journal of Volcanology and Geothermal Research, v. 26, p. 275–296.

Ibarra, Y., Corsetti, F.A., Cheetham, M.I., and Feakins, S.J., 2014, Were fossil spring-associated carbonates near Zaca Lake, Santa Barbara, California deposited under an ambient or thermal regime?: Sedimentary Geology, v. 301, p. 15–25.

Ibarra, Y., and Sanon, S., 2019, A freshwater analog for the production of *Epiphyton*-like microfossils: Geobiology, v. 17, p. 510–522.

Imlay, R.W., 1954, Marine Jurassic formation in the Pryor Mountains and northern Bighorn Mountains, Montana, *in* Williams, R.P., editor, Pryor Mountains-northern Bighorn Basin, Montana: Billings Geological Society 5th Annual Field Conference, p. 54–64.

Jansa, L., 1972, Depositional history of the coal-bearing Upper Jurassic–Lower Cretaceous Kootenay Formation, southern Rocky Mountains, Canada: Geological Society of America Bulletin, v. 83, p. 3199–3222.

Janssen, A., Swennen, R., Podoor, N., and Keppens, E., 1999, Biological and diagenetic influence in recent and fossil tufa deposits from Belgium: Sedimentology Geology, v. 126, p. 75–95.

Johnson, E.A., 2005, Geologic assessment of undiscovered oil and gas resources in the Phosphoria total petroleum system, southwestern Wyoming province, Wyoming, Colorado, Utah: U.S. Geological Survey Digital Data Series, DDS-69-D, p. 1–46.

Jones, B., and Renaut, R.W., 2010, Calcareous spring deposits in continental settings, *in* Alonso-Zarza, A.M., and Tanner, L.H., editors, Carbonates in continental settings facies, environments, and processes: Developments in Sedimentology, v. 61, p. 177–224.

Keppel, M.N., Clarke, J.D.A., Halihan, T., Love, A.J., and Werner, A.D., 2011, Mound springs in the arid Lake Eyre South region of South Australia—a new depositional tufa model and its controls: Sedimentary Geology, v. 240, p. 55–70.

Keppel, M.N., Post, V.E.A., Love, A.J., Clarke, J.D.A., and Werner, A.D., 2012, Influences on the carbonate hydrochemistry of mound spring environments, Lake Eyre South region, South Australia: Chemical Geology, v. 296–297, p. 50–65.

Kerney, M.P., 1959, An interglacial tufa near Hitchin, Hertfordshire: Proceedings of the Geologists' Association, v. 70, p. 322–337.

Khalid, M.E.A., 1990, Sedimentology of the Swift Formation (Jurassic) in the Little Rocky Mountains: Saskatoon, University of Saskatchewan, M.S. thesis, 107 p.

Koban, C.G., and Schweigert, G., 1993, Microbial origin of travertine fabrics—two examples from southern Germany (Pleistocene Stuttgart travertines and Miocene Riedöschingen travertine): Facies, v. 29, p. 251–264.

Linhart, C., and Schagerl, M., 2011, Autecology of the rare tufa-forming desmid *Oocardium stratum* Naeg: Austria, University of Vienna, Ph.D. dissertation, 86 p.

Loke, M.H., Chambers, J.E., Rucker, D.F., Kuras, O., and Wilkinson, P.B., 2013, Recent developments in the direct-current geoelectrical imaging method: Journal of Applied Geophysics, v. 95, p. 135–156.

Ludvigson, G.A., González, L.A., Fowle, D.A., Roberts, J.A., Driese, S.G., Villarreal, M.A., Smith, J.J., and Suarez, M.B., 2013, Paleoclimatic application and modern process studies of pedogenic siderite, *in* Driese, S.G., and Nordt, L.C., editors, New frontiers in paleopedology and terrestrial paleoclimatology—paleosols and soil surface analog systems: SEPM (Society for Sedimentary Geology) Special Publication 104, p. 79–87.

Mackenzie, F.T., and Pigott, J.D., 1981, Tectonic controls of Phanerozoic sedimentary rock cycling: Journal of the Geological Society of London, v. 138, p. 183–196.

Maughan, E.K., 1993, Stratigraphic and structural summary for central Montana, *in* Hunter, L.D.V., editor, Energy and mineral resources of central Montana: Montana Geological Society 1993 Field Conference Guidebook—Old Timers' Rendezvous Edition, p. 3–20.

Merz, M.U.E., 1992, The biology of carbonate precipitation by cyanobacteria: Facies, v. 26, p. 81–102.

Meyers, J.H., and Schwartz, R.K., 1994, Summary of depositional environments, paleogeography, and structural control on sedimentation in the Late Jurassic (Oxfordian) Sundance foreland basin, western Montana, *in* Caputo, M.V., Peterson, J.A., and Franczyk, K.J., editors, Mesozoic systems of the Rocky Mountain region, USA: SEPM (Society for Sedimentary Geology), p. 331–350.

Mohammadi, Z., Capezzuoli, E., Claes, H., Alipoor, R., Muchez, P., and Swennen, R., 2019, Substrate geology controlling different morphology, sedimentology, diagenesis and geochemistry of adjacent travertine bodies—a case study from the Sanandaj-Sirjan zone (western Iran): Sedimentary Geology, v. 389, p. 127–146.

Moore, D.M., and Reynolds, R.C., Jr., 1997, X-ray diffraction and the identification and analysis of clay minerals: New York, Oxford University Press, 378 p.

Müller, J., MacEachran, D., Burd, H., Sathitsuksanoh, N., Bi, C., Yeh, Y.-C., Lee, T.S., Hillson, N.J., Chhabra, S.R., Singer, S.W., and Bellerb, H.R., 2013, Engineering of *Ralstonia eutropha* H16 for autotrophic and heterotrophic production of methyl ketones: Applied and Environmental Microbiology, v. 79, p. 4433–4439.

Munoz-Saez, C., Saltiel, S., Manga, M., Nguyen, C., and Gonnermann, H., 2016, Physical and hydraulic properties of modern sinter deposits—El Tatio, Atacama: Journal of Volcanology and Geothermal Research, v. 325, p. 156–168.

Myers, T.S., Tabor, N.J., and Rosenau, N.A., 2014, Multiproxy approach reveals evidence of highly variable paleoprecipitation in the Upper Jurassic Morrison Formation (western United States): Geological Society of America Bulletin, v. 126, p. 1105–1116.

Nelson W.J., 1995, Basement control of recurrent faulting, central Montana: Basement Tectonics, v. 10, p. 265–282.

O'Neill, J.M., and Lopez, D.A., 1983, Great Falls lineament, Idaho and Montana [abs.]: American Association of Petroleum Geologists Bulletin, v. 67, no. 8, 1350–1351.

Park, R., and Epstein, S., 1961, Metabolic fractionation of C^{13} and C^{12} in plants: Plant Physiology, v. 36, p. 133–138.

Párraga, J., Rivadeneyra, M. A., Martín-García, J.M., Delgado, R., and Delgado, G., 2004, Precipitation of carbonates by bacteria from a saline soil, in natural and artificial soil extracts: Geomicrobiology Journal, v. 21, 55–66.

Parrish, J.T., Hasiotis, S.T., and Chan, M.A., 2017, Carbonate deposits in the Lower Jurassic Navajo Sandstone, southern Utah and northern Arizona U.S.A.: Journal of Sedimentary Research, v. 87, p. 740–762.

Parrish, J.T., Hyland, E.G., Chan, M.A., and Hasiotis, S.T., 2019, Stable and clumped isotopes in desert carbonate spring and lake deposits reveal palaeohydrology—a case study of the Lower Jurassic Navajo Sandstone, south-western USA: Sedimentology, v. 66, p. 32–52.

Parrish, J.T., and Peterson, F., 1988, Wind directions predicted from global circulation models and wind directions determined from eolian sandstones of the western United States—a comparison: Sedimentary Geology, v. 56, p. 261–282.

Parrish, J.T., Peterson, F., and Turner, C.E., 2004, Jurassic "savannah"—plant taphonomy and climate of the Morrison Formation (Upper Jurassic, Western USA): Sedimentary Geology, v. 167, p. 137–162.

Parrish, J.T., Ziegler, A.M., and Scotese, C.R., 1982, Rainfall patterns and the distribution of coals and evaporite in the Mesozoic and Cenozoic: Palaeogeography, Palaeoclimatology, Palaeoecology, v. 40, p. 67–101.

Pedley, H.M., 1990, Classification and environmental models of cool freshwater tufas: Sedimentary Geology, v. 68, p. 143–154.

Pedley, H.M., 2009, Tufas and travertines of the Mediterranean region—a testing ground for freshwater carbonate concepts and developments: Sedimentology, v. 56, p. 221–246.

Pentecost, A., 1990, The algal-flora of travertine—an overview, *in* Hermon, J.S., and Hubbard, D.A., editors, Travertine-marl—stream deposits in Virginia: Virginia Division of Mineral Resources Publication 101, p. 117-128.

Pentecost, A., 1991, A new and interesting site for the calcite-encrusted desmid *Oocardium stratum* Naeg. in the British Isles: British Phycological Journal, v. 26, p. 297–301.

Pentecost, A., 2005, Travertine: Heidelberg, Springer-Verlag Berlin, 445 p.

Pentecost, A., and Coletta, P., 2007, The role of photosynthesis and CO_2 evasion in travertine formation—a quantitative investigation at an important travertine-depositing hot spring, Le Zitelle, Lazio, Italy: Journal of the Geological Society, v. 164, p. 843–853.

Peterson, F., and Turner-Peterson, C.E., 1987, The Morrison Formation of the Colorado Plateau—recent advances in sedimentology, stratigraphy, and paleotectonics: Hunteria, v. 2, p. 1–18.

Pfiester, L.A., 1976, *Oocardium stratum* a rare (?) desmid (Chlorophyceae): Journal of Phycology, v. 12, p. 134.

Pipiringos, G.N., and O'Sullivan, R.B., 1978, Principal unconformities in Triassic and Jurassic rocks, Western Interior United States—a preliminary survey: U.S. Geological Survey Professional Paper 1035A, p. 1–29.

Ponder, W.F., 1986, Mound springs of the Great Artesian Basin: Limnology in Australia, p. 403–420.

Porter, J.R., 2011, Stratigraphic analysis of the Jurassic Ellis Group and paleotectonics in north-central Montana—deciphering the historically enigmatic "Belt Island:" Bozeman, Montana State University, M.S. thesis, 133 p.

Porter, K., Wheaton, J., and Miller, M., 2002, Potential for a public water supply from the Madison Limestone in the eastern Big Snowy Mountains and Little Snowy Mountains, Montana: Montana Bureau of Mines and Geology Open-File Report 449, p. 1–25.

Rees, P.M., Noto, C.R., Parrish, M.J., and Parrish, J.T., 2004, Late Jurassic climates, vegetation, and dinosaur distributions: Journal of Geology, v. 112, 643–653.

Rees, P.M., Ziegler, A.M., and Valdes, P.J., 2000, Jurassic phytogeography and climates—new data and model comparisons, *in* Huber, B.T., Macleod, K.G., and Wing, S.L., editors, Warm climates in earth history: Cambridge, Cambridge University Press, p. 297–318.

Renaut, R.W., and Jones, B., 2000, Microbial precipitates around continental hot springs and geysers, *in* Riding R.E., and Awramik, S.M., editors, Microbial sediments: Berlin, Springer, p. 187–195.

Richmond, D.R., Lukens, M.W., and Celestino, S.M., 2017, Upper Jurassic Morrison Formation clams on the half shell, central Montana [abs.]: Geological Society of America Abstracts with Programs, v. 49, no. 5, paper no. 4–2.

Richmond, D.R., Lupia, R., Philippe, M., and Klimek, J., 2019a, First occurrence of the boreal fossil wood *Xenoxylon meisteri* from the Jurassic of North America—Morrison Formation of central Montana, USA: Review of Palaeobotany and Palynology, v. 267, p. 39–53.

Richmond, D.R., Lupia, R., and Philippe, M., 2019b, First report of the fossil wood *Piceoxylon* from the North American Jurassic (Morrison Formation, central Montana) [abs.]: Geological Society of America Abstracts with Programs, 51, no. 2, p. 24, paper 38–12.

Richmond, D.R., Lupia, R., and Philippe, M., 2019c, *Circoporoxylon* from the Upper Jurassic Morrison Formation of central Montana [abs.]: Geological Society of America Abstracts with Programs, v. 51, no. 5, paper 271–15.

Richmond, D.R., and Murphy, N., 2017, Beach front property in central Montana—the Upper Jurassic Morrison Formation in the northern portion of the foreland basin [abs.]: American Association of Petroleum Geologists Search and Discovery Article #90301.

Richmond, D.R., and Murphy, N., 2020, Stratigraphy, sedimentology, and depositional facies of the Morrison Formation 5ES quarry of central Montana: Geological Society of America Abstracts with Programs, v. 52, no. 6, paper 3–12.

Richmond, D.R., Pigott, J., Lupia, R., Behm, M., and Hein, D., 2020, Subartesian carbonate mound spring deposits of the Upper Jurassic Morrison Formation of central Montana—paleo-precipitation proxies [abs.]: Geological Society of America Abstracts with Programs, v. 52, no. 6, paper 29-4.

Roden, E.E., McBeth, J.M., Blöthe, M., Percak-Dennett, E.M., Fleming, E.J., Holyoke, R.R., Luther, G.W., III, Emerson, D., and Schieber, J., 2012, The microbial ferrous wheel in a neutral pH groundwater seep: Frontiers in Microbiology, v. 3, p. 1–18.

Roden, E.E., Sobolev, D., Glazer, B., and Luther, G.W., 2004, Potential for microscale bacterial Fe redox cycling at the aerobic-anaerobic interface: Geomicrobiology Journal, v. 21, p. 379–391.

Ronholm, J., Schumann, D., Sapers, H.M., Izawa, M., Applin, D., Berg, B., Mann, P., Vali, H., Flemming, R.L., Cloutis, E.A., and Whyte, L.G., 2014, A mineralogical characterization of biogenic calcium carbonates precipitated by heterotrophic bacteria isolated from cryophilic polar regions: Geobiology, v. 12, p. 542–556.

Rott, E., Hotzy, R., Cantonati, M., and Sanders, D., 2012, Calcification types of *Oocardium stratum* Nägeli and microhabitat conditions in springs of the Alps: Freshwater Science, v. 31, p. 610–624.

Rouse, G.E., 1959, Plant microfossils from Kootenay coal-measures strata of British Columbia: Micropaleontology, v. 5, p. 303–324.

Saitta, E.T., 2015, Evidence for sexual dimorphism in the plated dinosaur *Stegosaurus mjosi* (Ornithischia, Stegosauria) from the Morrison Formation (Upper Jurassic) of Western USA: PLoS One, 10. e0123503. doi:10.1371/journal.pone.0123503.

Sanders, D., and Rott, E., 2009, Contrasting styles of calcification by the micro-alga *Oocardium stratum* Nägeli 1849 (Zygnematophyceae) in two limestone-precipitating spring creeks of the Alps: Austrian Journal of Earth Sciences, v. 102, p. 34–49.

Schuster, R.M., 1966, The Hepaticae and Anthocerotae of North America Vol. I.: New York, Columbia University Press, 801 p.

Selles-Martinez, J., 1994, New insights in the origin of cone-in-cone structures: Carbonates and Evaporites, v. 9, p. 172–186.

Sharp, Z., 2017, Principles of stable isotope geochemistry, 2nd Edition: University of New Mexico, doi: https://doi.org/10.25844/h9q1-0p82.

Shaw, J., and Renzaglia, K., 2004, Phylogeny and diversification of bryophytes: American Journal of Botany, v. 91, p. 1557–1581.

Sheldon, N.D., and Tabor, N.J., 2009, Quantitative paleoenvironmental and paleoclimatic reconstruction using paleosols: Earth-Science Reviews, v. 95, p. 1–52.

Silverman, A., and Harris, W.L., 1966, Economic geology of the Great Falls-Lewistown coal field west-central Montana, *in* Cox, J.E., editor, Jurassic and Cretaceous stratigraphic traps, Sweetgrass arch: Billings Geological Society 17th Annual Field Conference, 149–163.

Sims, P.K., O'Neill, J.M., Bankey, V., and Anderson, E., 2004, Precambrian basement geologic map of Montana—an interpretation of aeromagnetic anomalies: U.S. Geological Survey Scientific Investigations Map SIM-2829, 1 plate, scale 1:1,000,000.

Slessarev, E.W., Lin, Y., Bingham, N.L., Johnson, J.E., Dai, Y., Schimel, J.P., and Chadwick, O.A., 2016, Water balance creates a threshold in soil pH at the global scale: Nature, v. 540, p. 567–569.

Snee, L.W., Reynolds, M.W., and Miggins, D.P., 2002, Late Cretaceous and Tertiary plutonism, west-central Montana—pins in the end of compression and the beginning of extension [abs.]: Geological Society of America Abstracts with Programs, v. 34, no. 6, p. 43.

Springer, K.B., Pagati, J.S., and Scott, E., 2017, Geology and vertebrate taphonomy of Tule Spring Fossil Beds National Monument, Nevada, USA: Geological Society of America Field Guide 45, p. 1–30.

Steinen, R.P., Gray, N.H., and Mooney, J., 1987, A Mesozoic carbonate hot-spring deposit in the Hartford Basin of Connecticut: Journal of Sedimentary Petrology, v. 57, p. 319–326.

Tanner, L.H., 2010, Continental carbonates as indicators of paleoclimate: Developments in Sedimentology, v. 62, p. 179–214.

Terzer, S., Wassenaar, L.I., Araguás-Araguás, L.J., and Aggarwal, P.K., 2013, Global isoscapes for $\delta^{18}O$ and $\delta^{2}H$ in precipitation—improved prediction using regionalized climatic regression models: Hydrology and Earth Systems Science, v. 17, p. 1–16.

Tran, H., Rott, E., and Sanders, D., 2019, Exploring the niche of a highly effective biocalcifier—calcification of the eukaryotic microalga *Oocardium stratum* Nägeli 1849 in a spring stream of the Eastern Alps: Facies, v. 65, p. 1–24.

Turner, C.E., and Peterson, F., 1999, Biostratigraphy of dinosaurs in the Upper Jurassic Morrison Formation of the Western Interior, U.S.A., *in* Gillette, D.D., editor, Vertebrate paleontology in Utah: Utah Geological Survey Miscellaneous Publication 99-1, p. 77–114.

Turner, C.E., and Fishman, N.S., 1991, Jurassic Lake T'oo'dichi'—a large alkaline, saline lake, Morrison Formation, eastern Colorado Plateau: Geological Society of America Bulletin, v. 103, p. 538–558.

Turner-Peterson, C.E., and Fishman, N.S., 1986, Geologic synthesis and genetic models for Uranium mineralization in the Morrison Formation, Grants uranium region, New Mexico, *in* Turner-Peterson, C.E., and Santos, E.S., editors, A basin analysis case study—the Morrison Formation, Grants uranium regions, New Mexico: American Association of Petroleum Geologists Studies in Geology no. 22, p. 357–388.

Uhlir, D.M., Akers, A., and Vondra. C.F., 1988, Tidal inlet sequence, Sundance Formation (Upper Jurassic), north-central Wyoming: Sedimentology, v. 35, p. 739–752.

Valdes, P.J., and Sellwood, B.W., 1992, A palaeoclimate model for the Kimmeridgian: Palaeogeography, Palaeoclimatology, Palaeoecology, v. 95, p. 47–72.

Veizer, J., Ala, D., Azmy, K., Bruckschen, P., Buhl, D., Bruhn, F., Carden, G.A.F., Diener, A., Ebneth, S., Godderis, Y., Jasper, T., Korte, C., Pawellek, F., Podlaha, O.G., and Strauss, H., 1999, $^{87}Sr/^{86}Sr$, $\delta^{13}C$ and $\delta^{18}O$ evolution of Phanerozoic seawater: Chemical Geology, v. 161, p. 59–88.

Williams, A.F., and Holmes, J.W., 1978, A novel method of estimating the discharge of water from mound springs of the Great Artesian Basin, central Australia: Journal of Hydrology, v. 38, p. 263–272.